Spectral Properties of Type Ia Supernovae and Implications for Cosmology

Jakob Nordin

Stockholm University

Doctoral Thesis in Physics
Department of Physics
Stockholm University
Sweden

ISBN: 978-91-7447-300-1 (pp i–xii,1–83)

Printed by Universitetsservice US-AB, Stockholm, Sweden, 2011.

The cover includes the Union2 Hubble diagram [from 2], template Type Ia supernova lightcurves and a spectrum of supernova 20625 [SDSS ID; from Paper B].

Abstract

Type Ia supernovae can, for a short period of time, reach the same brightness as an entire galaxy. They are responsible for the creation of a large fraction of all heavy elements and can be used, as standard candles, to prove that the expansion of the universe is accelerating. Yet, we do not fully understand them.

A basic picture where Type Ia supernovae are caused by thermonuclear explosions of white dwarfs is generally accepted, but the details are still debated. These unknowns propagate into systematic uncertainties in the estimates of cosmological parameters. A Monte Carlo framework, `SMOCK`, designed to model this error propagation, is presented. Evolution with time/distance and the nature of reddening are studied as the dominant astrophysical uncertainties.

Optical spectra of Type Ia supernovae contain a wealth of information regarding the nature of these events, and can be used both to understand supernovae and to limit the systematic uncertainties in cosmological parameter estimates. We have reduced spectra observed with the Nordic Optical Telescope and the New Technology Telescope in conjunction with the SDSS-II supernova survey, and compared spectral properties (pseudo-Equivalent Widths and line velocities) of this sample with local supernovae. We have further studied possible systematic difficulties in such comparisons between nearby and distant supernovae, caused by noise and host galaxy contamination. Taking such uncertainties into account, we find a tentative evolution in supernova properties with redshift, compatible with expected demographic changes. Correlations with light curve shape found by other studies are confirmed. A tentative correlation with light curve colour is also presented. The latter could indicate an intrinsic component of the observed reddening, i.e. independent of interstellar dust in the host galaxy.

Accompanying Papers

This thesis is based on the following papers, which are referred to as Paper A to D in the text. The author's contribution to each paper is summarised below.

Paper A

Quantifying systematic uncertainties in supernova cosmology

J. Nordin, A. Goobar, J. Jönsson

Journal of Cosmology and Astroparticle Physics, Issue 02, 2008, pp. 008.

The author developed both the simulation framework presented and the analysis of systematic uncertainties in supernova cosmology. The author wrote most of the sections.

Paper B

NTT and NOT spectroscopy of SDSS-II supernovae

L. Östman, **J. Nordin**, A. Goobar, R. Amanullah, M. Smith, J. Sollerman, V. Stanishev, M.D. Stritzinger, B.A. Bassett, T.M. Davis, E. Edmondson, J. A. Frieman, P.M. Garnavich, H. Lampeitl, G. Leloudas, J. Marriner, R.C. Nichol, K. Romer, M. Sako, D.P. Schneider, C. Zheng

Astronomy and Astrophysics, Volume 526, 2011, id.A28.

The spectra from the NTT and NOT telescopes presented were reduced by the author together with L. Östman. The author developed the method for estimating the host galaxy contamination and wrote the sections describing this.

Paper C

Spectral properties of type Ia supernovae up to z ~ 0.3

J. Nordin, L. Östman, A. Goobar, R. Amanullah, R.C. Nichol, M. Smith, J. Sollerman, B.A. Bassett, J. Frieman, P.M. Garnavich, G. Leloudas, M. Sako, D.P. Schneider

Astronomy and Astrophysics, Volume 526, 2011, id.A119.

The author developed the algorithms used for automatic measurements of properties of SNe Ia spectra, as well as the methods for estimation of statistical and systematic uncertainties. The author led the analysis of spectral properties and wrote most of the sections.

Paper D

Evidence for a correlation between the Si II λ4000 width and Type Ia supernova color

J. Nordin, L. Östman, A. Goobar, C. Balland, H. Lampeitl, R. C. Nichol, M. Sako, D. P. Schneider, M. Smith, J. Sollerman, J. C. Wheeler

The Astrophysical Journal, in press, arXiv:astro-ph/1012.4430

The author initiated and constructed the analysis and wrote most of the text.

Additional Publications not Included in the Thesis

Spectra and Light Curves of Six Type Ia Supernovae at $0.511 < z < 1.12$ and the Union2 Compilation

R. Amanullah, C. Lidman, D. Rubin, G. Aldering, P. Astier, K. Barbary, M. S. Burns, A. Conley, K. S. Dawson, S. E. Deustua, M. Doi, S. Fabbro, L. Faccioli, H. K. Fakhouri, G. Folatelli, A. S. Fruchter, H. Furusawa, G. Garavini, G. Goldhaber, A. Goobar, D. E. Groom, I. Hook, D. A. Howell, N. Kashikawa, A. G. Kim, R. A. Knop, M. Kowalski, E. Linder, J. Meyers, T. Morokuma, S. Nobili, **J. Nordin**, P. E. Nugent, L. Ostman, R. Pain, N. Panagia, S. Perlmutter, J. Raux, P. Ruiz-Lapuente, A. L. Spadafora, M. Strovink, N. Suzuki, L. Wang, W. M. Wood-Vasey, N. Yasuda (Supernova Cosmology Project)

The Astrophysical Journal, Volume 716, Issue 1, pp. 712-738 (2010).

Measurements of the Rate of Type Ia Supernovae at Redshift $z <\sim 0.3$ from the SDSS-II Supernova Survey

B. Dilday, M. Smith, B. Bassett, A. Becker, R. Bender, F. Castander, D. Cinabro, A.V. Filippenko, J.A. Frieman, L. Galbany, P.M. Garnavich, A. Goobar, U. Hopp, Y. Ihara, S.W. Jha, R. Kessler, H. Lampeitl, J. Marriner, R. Miquel, M. Molla, R.C. Nichol, **J. Nordin**, A.G. Riess, M. Sako, D.P. Schneider, J. Sollerman, J.C. Wheeler, L. Östman, D. Bizyaev, H. Brewington, E. Malanushenko, V. Malanushenko, D. Oravetz, K. Pan, A. Simmons, S. Snedden

The Astrophysical Journal, Volume 713, Issue 2, pp. 1026-1036 (2010).

A Measurement of the Rate of Type Ia Supernovae in Galaxy Clusters from the SDSS-II Supernova Survey

B. Dilday, B. Bassett, A. Becker, R. Bender, F. Castander, D. Cinabro, J.A. Frieman, L. Galbany, P. Garnavich, A. Goobar, U. Hopp, Y. Ihara, S.W. Jha, R. Kessler, H. Lampeitl, J. Marriner, R. Miquel, M. Mollá, R.C. Nichol, **J. Nordin**, A.G. Riess, M. Sako, D.P. Schneider, M. Smith, J. Sollerman, J.C. Wheeler, L. Östman, D. Bizyaev, H. Brewington, E. Malanushenko, V. Malanushenko, D. Oravetz, K. Pan, A. Simmons, S. Snedden

The Astrophysical Journal, Volume 715, Issue 2, pp. 1021-1035 (2010).

Type II-P Supernovae from the SDSS-II Supernova Survey and the Standardized Candle Method

C.B. D'Andrea, M. Sako, B. Dilday, J.A. Frieman, J. Holtzman, R. Kessler, K. Konishi, D.P. Schneider, J. Sollerman, J.C. Wheeler, N. Yasuda, D. Cinabro, S. Jha, R.C. Nichol, H. Lampeitl, M. Smith, D.W. Atlee, B. Basset, F.J. Castander, A. Goobar, R. Miquel, **J. Nordin**, L. Östman, J.L. Prieto, R. Quimby, A.G. Riess, M. Stritzinger

The Astrophysical Journal, Volume 708, Issue 1, pp. 661-674 (2010).

The Effect of Host Galaxies on Type Ia Supernovae in the SDSS-II Supernova Survey

H. Lampeitl, M. Smith, R.C. Nichol, B. Bassett, D. Cinabro, B. Dilday, R.J. Foley, J.A. Frieman, P.M. Garnavich, A. Goobar, M. Im, S.W. Jha, J. Marriner, R. Miquel, **J. Nordin**, L. Östman, A.G. Riess, M. Sako, D.P. Schneider, J. Sollerman, M. Stritzinger

The Astrophysical Journal, Volume 722, Issue 1, pp. 566-576 (2010).

Common abbreviations

DAR	Differential Atmospheric Refraction
FLRW	Friedmann-Lemaitre-Robertson-Walker (metric)
NOT	Nordic Optical Telescope
NTT	New Technology Telescope
PSF	Point Spread Function
PCA	Principal Component Analysis
S/N	Signal-to-Noise
SDSS	Sloan Digital Sky Survey
SED	Spectral Energy Distribution
SN	Supernova
SNe	Supernovae
SN Ia	Type Ia supernova
WD	White Dwarf
C+O WD	Carbon-Oxygen White Dwarf

Contents

Chapter 1

Introduction

A decade ago the way we view the cosmos was fundamentally altered: it was shown that the expansion of the universe is accelerating, powered by an until that time unknown energy source, *dark energy*. This expansion was detected using *Type Ia supernovae* (SNe Ia), extremely bright exploding stars [95, 102].

Today the existence of dark energy has been confirmed using a range of different techniques. But we still have little knowledge regarding its properties. At the same time there are many unanswered questions regarding SNe Ia as astrophysical objects.

This thesis concerns these topics: How can we use supernovae to obtain better constraints on dark energy properties? And what is it really that explodes?

Chapter 4 (Paper A) shows that these questions are closely related: to understand dark energy we need to understand SNe Ia. Chapter 5 (Paper B) and Chapter 6 (Papers C and D) will introduce the NTT/NOT SDSS spectroscopic sample and use this to probe the nature of SNe Ia. Using spectroscopic indicators we study evolution with time as well as connections with reddening and host galaxy properties, some current major SNe Ia unknowns.

Before this, Chapter 2 introduces general relativity, the theory describing the expanding universe, and Chapter 3 summarises our current understanding of SNe Ia. Finally, results are collected and possible continued work based on this thesis is discussed in Chapter 7. Chapter 8 lists some common astronomical terms.

A description of the content of this thesis for the general public can be found in Chapter 9.

Chapter 2

General Relativity and Cosmology

This Chapter introduces the theoretical framework used when studying the universe. Equations and implications will only be stated here. Many more complete texts on general relativity at different levels exist [e.g. 12, 121]. The goal is to introduce *standard candles* as a tool to probe the expansion history of the universe.

2.1 General Relativity

Einstein noted that it is impossible for an observer to locally distinguish between constant acceleration and attraction by gravity (*the equivalence principle*). Since we cannot distinguish these situations the laws of nature should connect them. Similarly we can view a satellite orbiting a massive object as freely falling but along a path curved by the nearby mass. We must thus have some connection between matter/energy and how things move.

Matter and energy can be conveniently described using the *stress-energy tensor* $T_{\mu\nu}$ where the μ and ν indices can take any of four values 0,1,2 or 3 (time+three spatial).[1] A fundamental property of $T_{\mu\nu}$ is that it, through construction, is symmetric ($T_{\mu\nu} = T_{\nu\mu}$) and divergenceless ($\nabla_\nu T^{\mu\nu} = 0$). The task motivated by the equivalence principle can thus be reformulated as: how can properties of space and time be connected to $T_{\mu\nu}$?

We are used to calculate a distance (ds) as $ds^2 = dx^2 + dy^2 + dz^2$. This is only true in a flat space. In a possibly curved space this gets modified:

[1] The components of $T_{\mu\nu}$ can be described as flow in μ direction of ν-direction momentum where energy is momentum in the time direction (0).

$ds^2 = g_{xx}dx^2 + g_{yy}dy^2 + g_{zz}dz^2 + g_{xy}dxdy + g_{yx}dydx + g_{xz}dxdz + g_{zx}dzdx + g_{zy}dzdy + g_{yz}dydz = g_{ij}dx^i dx^j$. The last step introduces the convenient tensor formulation where repeated indices (here i and j) should be summed over all dimensions (here x,y,z). If a fourth dimension, time, is introduced, a general distance between two points can be written $ds^2 = g_{\mu\nu}dx^\mu dx^\nu$ where μ and ν range over (t,x,y,z). Spacetime, being a collection of space and time distances, can now be described using the elements of the tensor $g_{\mu\nu}$ - the *metric*.

We thus want to connect the metric with $T_{\mu\nu}$. Einstein showed that only one symmetric and divergenceless combination of the metric exists. This is now called the Einstein tensor:

$$G_{\mu\nu} = R_{\mu\nu} - \frac{1}{2}g_{\mu\nu}R \tag{2.1}$$

where $R = g^{\mu\nu}R_{\mu\nu}$, $R_{\mu\nu} = R^\alpha_{\mu\alpha\nu}$ and $R^\sigma_{\mu\alpha\nu}$ is the Riemann curvature tensor. The latter is a complicated object, but created from the metric $g_{\mu\nu}$ and its derivatives in a straightforward process. We must therefore have $G_{\mu\nu} = constant \cdot T_{\mu\nu}$.

If we finally demand that this equation reduces to Newtonian gravity in the limit of weak gravity, the constant can be determined and we find Einsteins equations of general relativity:

$$R_{\mu\nu} - \frac{1}{2}g_{\mu\nu}R = 8\pi G_N T_{\mu\nu}. \tag{2.2}$$

2.2 Cosmology

Einsteins equations are very compact and beautiful. They are also very complex and difficult to solve - to do so simplifying assumptions have to made. Since the universe at large scales looks very similar we can assume that it is *homogeneous*. If we further assume that earth does not occupy a special position (and thus any observer at any point would observe a similar universe) we find *isotropy*. We will finally assume that the energy content of the universe can be described as a perfect fluid ($T_{00} = \rho$, $T_{ii} = p$, $\rho = density$, $p = pressure$, all other $T_{\mu\nu} = 0$).

With these assumptions we can first express the spacetime metric in a simple way (using units where $c = 1$):

$$ds^2 = dt^2 - a^2(t)[dr^2/(1 - kr^2) + r^2 d\theta^2 + r^2 \sin^2\theta d\phi^2], \tag{2.3}$$

where (r, θ, ϕ) are (comoving) spatial coordinates, t time, k the curvature of the universe and a the scale factor describing the expansion of the universe. By convention $a = 1$ today. This is the Friedmann-Lemaitre-Robertson-Walker (FLRW) metric. If the FLRW metric is applied to Einsteins equations, Equation 2.2, these reduce to the Friedmann equations:

$$H^2 = \left(\frac{\dot{a}}{a}\right)^2 = \frac{8\pi G\rho}{3} - \frac{k}{a^2} \tag{2.4}$$

$$\frac{\ddot{a}}{a} = -\frac{4\pi G}{3}(\rho + 3p), \tag{2.5}$$

where ρ is the total energy density of the Universe, p the total pressure and H the *Hubble parameter*, defined as $H = \dot{a}/a$ (the value of the Hubble parameter today will be denoted H_0). We will here assume a flat universe (which CMB measurements have shown is true to a good precision), thus setting $k = 0$. Both density and pressure are sums over all components of the cosmic fluid: radiation, matter and a possible extra component: dark energy (DE). For each of these the equation-of-state parameter can be defined as $w_i \equiv p_i/\rho_i$. For constant w_i, the energy density for some scale factor a will be

$$\rho = \rho_0 a^{-3(1+w)} \tag{2.6}$$

where ρ_0 is the current energy density. Using the Hubble parameter, the critical density $\rho_c = 3H_0/8\pi G$, and the normalised densities $\Omega_i \equiv \rho_0^i/\rho_c$ (where the i index spans all relevant energy sources, $i = (M, r, DE)$ for matter, radiation or dark energy), Equation 2.4 can be rewritten

$$H^2 = H_0^2[\Omega_M(1+z)^3 + \Omega_r(1+z)^4 + \Omega_{DE}f(z)], \tag{2.7}$$

where

$$f(z) = (1+z)^{3(1+w_{DE})} \tag{2.8}$$

if assuming a *constant* dark energy equation of state. The z parameter is the *redshift*, zero today and increasing at higher distances.[2] The Ω_i parameters are examples of *cosmological parameters*, they determine both how the universe has and will evolve.The radiation energy density is negligible compared to the other components today, and can be neglected. If we set

[2]See Chapter 8 for a definition of *redshift*.

$w_{DE} = -1$, dark energy looses its redshift dependence and we get a constant density, called *the cosmological constant* Λ. Equation 2.7 then reduces to

$$H^2 = H_0^2[\Omega_M(1+z)^3 + \Omega_\Lambda]. \tag{2.9}$$

Through this formula it is clear that measurements of H yield constraints on cosmological parameters. For a light ray, $ds^2 = 0$ and we can write a distance r to a source as a function of its redshift z:

$$r(z) = \int_{observer}^{source} dr = \int_1^2 \frac{dt}{a} = \int_1^2 \frac{da}{a\dot{a}} = \int_0^z \frac{dz\prime}{H(z\prime)}. \tag{2.10}$$

Different cosmological parameters implies different $H(z\prime)$, and thus different distances $r(z)$. With $r(z)$, new "sorts" of distances (besides redshift) can be defined. We will here use the *luminosity distance* d_L, the "equivalent" distance in a Euclidean static universe, defined as

$$d_L(z) = (1+z)r(z).^3 \tag{2.11}$$

For an astronomical object, the relation between the intrinsic luminosity L and the observed flux F is

$$F = \frac{L}{4\pi d_L^2}. \tag{2.12}$$

Standard candles Objects with constant luminosity L are called *standard candles*. If we observe several such at different distances (different F), the change in d_L can be calculated as a function of z (which is separately measured). $d_L(z)$ is, in turn, sensitive to the integral of the Hubble parameter, as described above. In Chapter 4, after a discussion of Type Ia supernovae as standard candles, we will study the practical application of d_L measurements.

Alternative cosmological framework If we, as above, assume a cosmological constant, Λ, we have the so called ΛCDM model, which is both mathematically simple and provides excellent fit to current data. It is, however, mainly an empirical fit to data and not motivated by fundamental physics.[4] Λ also demands some fundamental assumptions: isotropy, homogeneity and that dark energy can be correctly described as a constant. A

[3] We will thus not make use of e.g. *angular distances*.

[4] Quantum field theory can be interpreted to imply the existence of a vacuum energy density, but ~ 120 orders of magnitude larger than what is observed.

large range of different alternative cosmological models exist, where the dark energy equation does not need to be constant (or where some of the other assumptions are relaxed). Since one of the fundamental questions regarding dark energy is whether some change in time exists, an immediate extension of the theory is to add some degree of redshift dependence to the dark energy component. This could, as suggested by e.g. Linder [83], be parametrised as

$$w_{DE} = w_0 + w_a z/(1+z), \tag{2.13}$$

which will lead to a modification of Equation 2.8:

$$f(z) = \exp\left[3\int_0^z dz\prime \frac{1+w_{DE}(z\prime)}{1+z\prime}\right]. \tag{2.14}$$

This parametrisation will be used below, where we fit for the parameters w_0 and w_a as an alternative to Ω_Λ.

Chapter 3

Type Ia Supernovae

This chapter introduces the astronomical objects called *Type Ia supernovae* (SNe Ia). These are extremely bright transient phenomena that are found to form a very homogeneous class of objects - they are almost perfect standard candles. The currently most popular explanation for their homogeneity and how this translates to the observed properties will be outlined.

3.1 Stars and Supernovae

Stars are formed through gravitational contraction of gas clouds, mainly consisting of hydrogen and helium. As the cloud cools down a rotating disk, with a central core, is formed. Friction in the core gas causes the temperature to increase. If the gas cloud is massive enough temperatures reach $\sim 1.5 \cdot 10^7$ K. At these temperatures the hydrogen in the now hot compressed gas can be fused into helium. Radiation is emitted in this process and photons slowly escape the surrounding colder material. A star is born.

Eventually the supply of hydrogen in the core of the star is exhausted. The outward radiation pressure necessary to resist the inward gravitational pressure can now be created through fusion of helium.[1] Energy can in this way be created through fusion of all elements lighter than iron. However, higher and higher temperatures are needed to fuse heavier elements. Helium fusion into carbon and oxygen can begin at temperatures around $\sim 10^8$ K.

The next burning stage, that of carbon and oxygen, demands a temperature of around 10^9 K, which in turn requires the mass of the star to exceed $8 - 10$ solar masses (often denoted $M_\odot$). For such very massive

[1] Very small non-massive stars might not be able to burn helium. However, these would have a lifetime exceeding that of the universe and quietly burn their hydrogen.

stars, increasingly heavy elements are thus created. Surrounding a core of iron group elements (Fe,Co,Ni) are layers of less heavy burning products (Si,O,Ne,C,He,H). When no more material can be fused and no energy is produced, nothing can counteract the gravitational force and the core will collapse. The collapse transforms the central core to a neutron star or black hole while creating a shock-wave propagating outwards, disrupting the outer part of the star. After reaching the surface, photons can propagate and be observed by us as a supernova. These supernovae show a large variation e.g. depending on mass, circumstellar material or whether outer hydrogen or helium layers still exist. Core collapse SNe are observationally divided into supernovae of Type II, Ib or Ic - anything *but* Type Ia!

For less massive stars (masses below $M < 8 - 10\,M_\odot$), no such violent collapse can take place. Hydrogen and helium are burned into carbon and oxygen as above (these are created in roughly equal proportions), but no further burning takes place since temperatures are too low. The outer hydrogen and helium envelopes are probably lost in the *Red giant* evolution stage. This leaves a small carbon-oxygen (C+O) core, a *white dwarf* (WD). These are very numerous (as the number of stars increases sharply with decreasing mass) but are too faint to be observed unless they are very nearby. The evolution of stars is described in a multitude of text books [e.g. 51].

Basic physical principles regulate the properties of C+O white dwarfs. According to the Pauli exclusion principle two fermions cannot occupy the same quantum state at the same time. This means that a degenerate fermion gas resists further compression and thus acts as a force preventing complete gravitational collapse. Once the WD runs out of radiation pressure created through nuclear burning, electron degeneracy pressure can still support the star.[2] But there is a fundamental limit, the *Chandrasekhar mass*, for how much mass can be supported. See [23] for the original derivation, but the reasoning can be simplified [from 39]:

For the degenerate Fermi gas we can approximate the pressure by

$$P \approx \frac{1}{3} n_e p v, \tag{3.1}$$

where n_e is the density, v the velocity and p the momentum of the electrons. The momentum can be estimated through the uncertainty relation $\Delta p \Delta x \approx \hbar$ and the electron density $n_e \approx 1/\Delta x^3$. Equation 3.1 thus becomes

$$P \approx \frac{1}{3} \hbar n_e^{4/3} v. \tag{3.2}$$

[2]The pressure caused by nucleons is very small in comparison.

Starting with the case where the electrons are **non-relativistic** and if we approximate the velocity through the uncertainty relation ($v \approx \hbar n_e^{1/3}/m_e$), we get

$$P \approx \frac{1}{3}\frac{\hbar^2}{m_e} n_e^{5/3}. \tag{3.3}$$

At the same time the pressure can be approximated through the hydrostatic equilibrium equations

$$\frac{dP}{dr} = -\frac{Gm(r)\rho}{r^2} \rightarrow P \approx \frac{GM\rho}{r} \approx GM^{2/3}\rho^{4/3}, \tag{3.4}$$

where that $\rho \approx 3M/(4\pi R^3)$ was used in the last step. Finally the electron density can be rewritten $n_e = Z\rho/Am_p$ (Z is the atomic number or number of protons, A the mass number and m_p the mass of the proton). Using the last two equations we get a relation between mass and density, or mass and radius, for the non-relativistic case:

$$R \propto M^{-1/3} \tag{3.5}$$

With increasing mass the radius thus decreases and the density increases. Eventually the electrons become relativistic (at $\sim 10^6\,\mathrm{g\,cm^{-3}}$). We thus need to consider the **relativistic** case, where $v = c$ and Equation 3.2 can be written

$$P \approx \frac{1}{3}\hbar n_e^{4/3} c \tag{3.6}$$

Combining this with Equation 3.4 we get an expression for the *Chandrasekhar mass*, independent of radius:

$$M_{Ch} \approx \left(\frac{c\hbar}{G}\right)^{3/2} \left(\frac{Z}{Am_p}\right)^2. \tag{3.7}$$

The full calculation yields numerical values such that, with $Z/A = 0.5$, $M_{Ch} = 1.46 M_\odot$. This is thus the mass of an object where the Fermi gas is completely degenerate and "squeezed" into smallest possible volume.[3] If the mass of a less massive object is increased, it will gradually approach full degeneracy and the Chandrasekhar mass limit. Assuming the increase continues to a mass above M_{Ch}, the star will no longer be supported against gravity, causing pressure to increase until nuclear burning can start. Since

[3] This mass can likely be slightly modified by including effects from e.g. rotation.

the thermal pressure is low (the star is supported by the electron pressure) the created heat feeds further nuclear burning instead of expansion. A thermonuclear runaway sets in, completely disrupting the star and burning elements to nuclear statistical equilibrium. A main product of such burning is the radioactive ^{56}Ni isotope.[4]

Such a system, an exploding C+O WD at the Chandrasekhar mass would be very simple, determined by very few parameters. The observed luminosities should be fairly uniform, not much hydrogen should be detectable and a sizable fraction of radioactive material should be created (where the emitted radiation declines in proportion to the radioactivity time scales). Finally, neutrinos would not carry away a large fraction of the energy (as is the case for core collapse SNe), allowing these SNe to emit a lot of energy at optically detectable wavelengths.

We now ask whether these WDs, increasing in mass, can be expected to be found. Two mechanisms for this have been suggested: the single and double degenerate scenarios. Both are based on the fact that many stars exist in binary pairs.

An accreting White Dwarf - single degenerate Stars in binary pairs often evolve at different speeds. One could thus shrink to a WD while the companion experiences a giant phase with strong winds, allowing mass to be transferred from the giant to the WD (left panel of Figure 3.1). Many stars are found in binary systems and it is thus not unlikely that a fair number of pairs should exist where the WD experiences exactly such mass transfer. Observational signatures of this explosion channel could be signs of the material being transferred from the companion or from the supernova ejecta interacting with the companion star [68]. However, thorough searches have detected neither H_α [28, 87] nor light curve distortions from interaction with a companion[54], putting limits on the size and nature of the companion star [these are, however, still debated, see e.g. 31, 67].

Two merging White Dwarfs - double degenerate Another viable explosion mechanism would be two binary stars that merge after having both evolved into the WD stage (right panel of Figure 3.1). This would explain why no signs of mass transfer have been detected and provide a natural mechanism for *Super Chandrasekhar-mass* SNe Ia (overluminous SNe Ia that possibly demand a progenitor mass larger than M_{Ch}, see Section 3.2.3). Further, the *Delay Time Distribution* (the distribution of time-lapses between

[4]Nickel with two neutrons less than the most common isotope, ^{58}Ni.

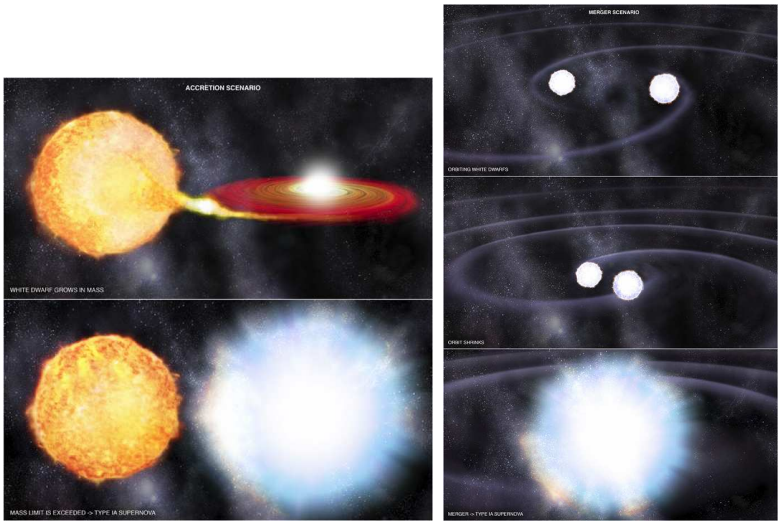

Figure 3.1: *Left panel:* A WD accreting mass from a companion star. "Artists image" *Right panel:* Two WDs merging. "Artists image" (Credit NASA/CXC/M.Weiss)

star formation and SN detonation) seems to be a fairly shallow declining function of time, more similar to what double degenerate, rather than single degenerate, models predict [8]. However, no conclusive evidence for any of the explosion channels exists. It is possible SNe Ia are produced through both channels.

A promising path for understanding astrophysical processes is through computer simulations. If scenarios such as those above can be accurately simulated and the output compared with observations we can hope to rule out false models. However, SNe Ia are extremely hard to model: Very complex explosion processes with large temperature gradients and fundamental 3D effects make any models very computationally demanding. A basic question is whether the burning front propagates as a subsonic (deflagration, lower than the speed of sound) or a supersonic (detonation) wave. In deflagration scenarios the WD has time to expand before being completely burned, leaving some fraction of both unburned C and O and partially burned Si, S and Ca. In a detonation, the complete WD should be burned to nuclear statistical equilibrium, leaving only iron peak elements. Since observations show some intermediate mass elements in the outer layers but hardly any in the centre, some expanding deflagration-like phase seems

to be required, while the inner layers are completely burned like after a detonation. Unburned carbon has been firmly detected only in a few early-epoch spectra [118].

A general review of models is given by Hillebrandt and Niemeyer [57]. To model an observed spectrum, radiative transfer codes, propagating the light from a basic explosion model through the outer layers of the ejecta, are used [108, 126]. Three dimensional effects, like clumping, seem necessary to match observations [75, 105].

3.2 Observations of Type Ia SNe

Supernovae were first classified as Type I (without obvious hydrogen in spectra) or Type II (with hydrogen) [89]. It was later ($\sim$ 1985) realised that Type I can be further divided into type Ia (showing Silicon absorption), type Ib (signs of Helium) and type Ic (neither Si or He) [33]. Type II, Ib and Ic probably all originate in core collapses of massive stars but differ in how the outer regions of the star are composed. There are examples of SNe gradually mutating between these types [e.g. SN1993J; see 34, 116]. Type Ia SNe constitute a completely different subclass. They are very homogeneous, showing no signs of hydrogen and are very bright, reaching a peak brightness of $M_B \sim -19.3$ magnitudes in the B band [52, 53].[5] This corresponds to $\sim 10^{10} L_\odot$, that is comparable to the luminosity of an entire galaxy (for a very short period).[6] Further, no compact objects have been detected at the positions of known Type Ia SNe, indicating that the complete star is disrupted [57]. Finally, their brightness declines at an exponential rate typical of energy deposits from radioactive decay.

These observations match very well with the theoretical expectations given above. We thus have reason to believe that these events really are the optical signatures of the thermonuclear disruption of C+O white dwarf(s) with masses at the Chandrasekhar limit.

3.2.1 Light Curve

The light curves of Type Ia SNe, that is the evolution of the luminosity in one or more photometric filters, are very similar.[7] The energy visible in optical bands quickly rises and reach maximum brightness around 20 days after the

[5] See Chapter 8 for a definition of *magnitude, band*.

[6] $L_\odot$ = luminosity of the sun.

[7] See Chapter 8 for a definition of *photometric filter*.

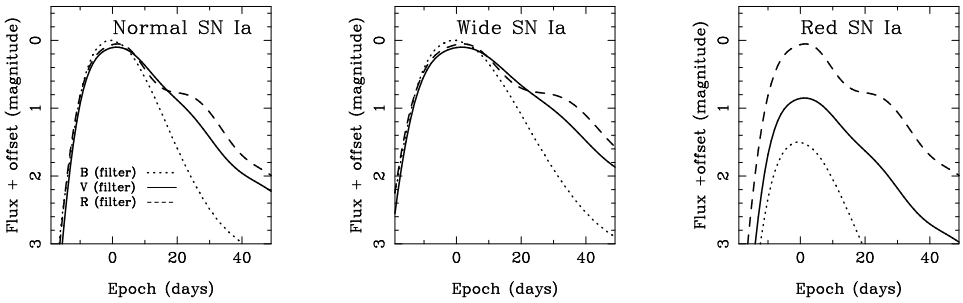

Figure 3.2: *Standardisable SN Ia light curves. Left panel:* Normal SN, in three filters. *Mid panel:* A "slow declining" SN with a wide "stretched" light curve. Such SNe are found to be brighter than normal SNe Ia. *Right panel:* A "reddened" SN, having relatively more flux in filters in higher wavelength regions. Such SNe are found to be less bright than normal SNe.

explosion. After this the luminosity gradually decreases exponentially, but with slightly different pattern for different filters. A shoulder can often be seen in near-IR wavelengths, likely related to opacity effects [59].

The exponential decline is typical of light emission powered by radioactive decay. The nuclear fusion in the explosion converts carbon and oxygen into ^{56}Ni, which decays via ^{56}Co into stable ^{56}Fe (roughly $\sim 0.5 M_\odot$ of ^{56}Ni is produced). Each of these steps produces energetic γ-rays that power the light curve when they are subsequently absorbed and reemitted as lower energy optical photons.

Standardisation through light curve properties

Standard candles are objects with small dispersion in their luminosities. What makes Type Ia SNe usable as standard candles, or rather standardisable candles, is the correlation between light curve shape and peak brightness. Without corrections peak luminosities show dispersions around 0.3 magnitudes, making their immediate use as standard candles limited. In 1993 Phillips [96] (continued in Hamuy et al. [52]) demonstrated observationally how the supernova light curve width correlates strongly with total luminosity: SNe with wider light curves are brighter. This thus allows *standardisation* of the luminosity, creating a very sharp standard candle and opening the field of Supernova Cosmology. The correlation can be well explained if SNe with more than average ^{56}Ni generated are both brighter and have wider light curves [3, 27, 88, 120]. In Figure 3.2 we sketch different light curve shapes.

Tripp [119] later demonstrated that the dispersion can be even further reduced by using the supernova colour [see also 98].[8] A red supernova, with relatively more flux at higher wavelengths, is on average fainter (See Figure 3.2). This can, for example, be characterised as the difference between the B and V rest frame filter magnitudes.[9] This difference, after the intrinsic SN colour has been subtracted, is usually called the colour excess $E(B-V)$.[10] A SN with large $E(B-V)$ is often called "reddened". A typical phenomenon causing such reddening is absorption by dust - more light is absorbed in bluer wavelengths thus creating a tilt of the spectrum [22], reducing flux in "bluer" filters. Whether all reddening is caused by dust alone is still not determined - we will return to this question in Chapter 6.

If corrections to both light curve width and colour are made the dispersion reduces to ~ 0.13 magnitudes, corresponding to $\sim 7\%$ in distance [5]. It now seems likely that SNe Ia can, at least in principle, be even further standardised. Using very well measured nearby SNe, Folatelli et al. [37] suggest that their dispersion is limited by host galaxy peculiar velocities and that the intrinsic SN distance dispersion is only 3-4%.

3.2.2 Optical Spectrum

A SN Ia spectrum can be broadly understood as caused by an expanding hot *photosphere* (the "deepest" layer seen) surrounded by layers of less dense material.[11] The dense photosphere emits thermalized black-body shaped light ($I(\lambda) \propto \lambda^{-5}(e^{hc/\lambda kT} - 1)^{-1}$). This gets absorbed and reemitted by the surrounding material. The fast expansion creates wide over-lapping (P-Cygni) absorption features. These steps are shown in Figure 3.3. Early spectra are dominated by wide absorption regions attributed to neutral or singly ionised intermediate mass elements (O, Mg, Si, S, Ca), with possibly some iron-group elements.

As the ejecta expands and cools, the photosphere recedes inwards and deeper layers are seen. The contributions from Fe-group elements quickly increase (FeII, FeIII, CoIII). That the late Type Ia spectra are dominated by iron shows that the core has gone through more or less complete burning to nuclear statistical equilibrium. Eventually the photosphere is completely

[8] See Chapter 8 for a definition of *colour*.

[9] See Chapter 8 for a definition of *rest frame*.

[10] Dust properties are often parametrised using the *total-to-selective* extinction ratio $R_V = A_V/E(B-V)$ where A_V is the extinction in the V filter and $E(B-V)$ the colour excess. Different R_V values then correspond to different types of dust.

[11] See Chapter 8 for a definition of *spectrum*.

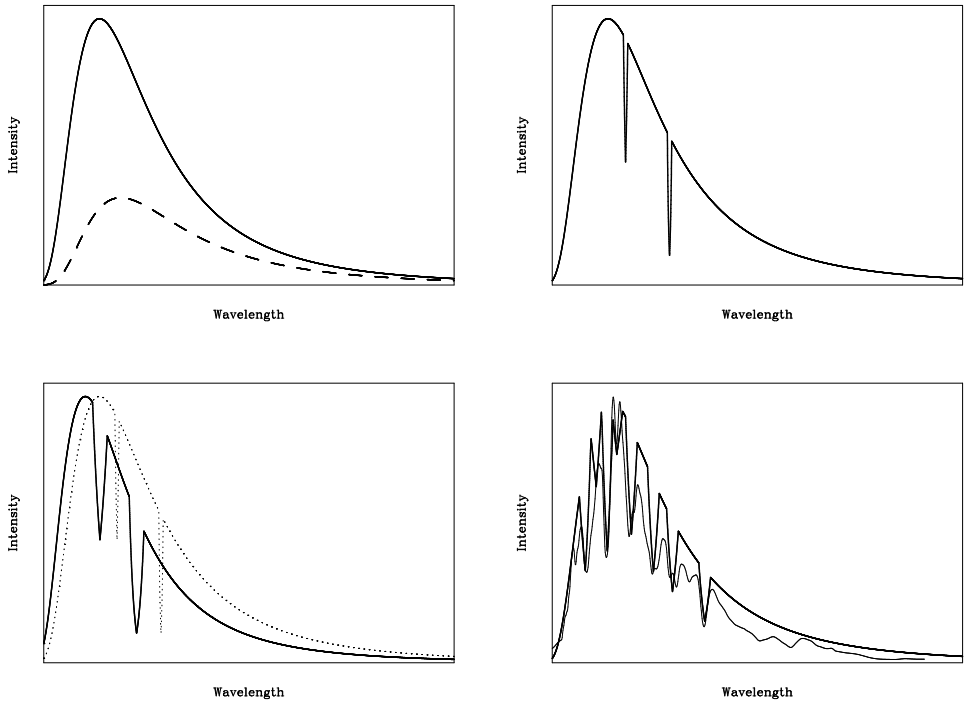

Figure 3.3: *Creation of a SN Ia spectrum. Top left:* Thermalized photons at the photosphere cause a black-body shaped spectrum at a specific temperature. Solid line showing a higher temperature black-body compared to dashed curve. *Top right:* An element outside the photosphere absorb photons at characteristic wavelengths. *Bottom left:* If a sphere of absorbing material expands towards us we will get blueshifted absorption. Further, absorbing elements at slightly different angles cause a widened absorption pattern. Often (but not included in Figure!) this causes a P-Cygni profile where the absorbed material resubmits at the rest frame wavelength. *Bottom right:* Adding absorption from multiple elements will cause the observed spectrum. Very fast expanding ejecta will cause lines to overlap. Thin line shows a SN Ia template spectrum [from 64] for comparison.

gone and only the emission lines of the nebular phase are seen. See [33] for a detailed description of optical spectra.

Compared with other types of SNe, the Type Ia SN spectrum is mainly characterised by not having any signs of H or He (the most abundant elements in the universe) but instead clear SiII absorptions, most notably around 6150 Å (lines blueshifted from $\lambda\lambda 6347, 6371$).

We will frequently use the term *epoch* of a SN Ia spectrum, with this we mean the difference in days between the time of light curve max (*in the B-band filter*) and the time of the spectrum observation, in the rest frame of the supernova. Type Ia supernova template spectra from four different epochs, showing the evolution with time, can be found in the left panel of Figure 3.4. It is clear that the amount of flux covered by e.g. a B-filter will change in time, yielding the light curves shown in Figure 3.2.

3.2.3 Subtypes of SNe Ia

Most SNe Ia form a very homogeneous class, but as more and more are observed a number of subclasses of more or less peculiar types have emerged. The two earliest studied such are the overluminous SN 1991T-like SNe [99] and the underluminous SN 1991bg-like SNe [35, 117]. These can (at least to some extent) be standardised along normal SNe and therefore be used for cosmology. It is not yet determined whether they form distinct subtypes or are part of a continuously changing population.

There are also "truly peculiar" SNe. This includes *over-Chandrasekhar mass events* like SN 2003fg [62], SN 2006gz [55] or SN 2007if [109]. These are so luminous that they seem to be powered by more ^{56}Ni than what can reasonably be created from a standard Chandrasekhar mass WD.

There is also a class of underluminous slow expanding SNe, including SN 2002cx and SN 2005hk, that must be created in a significantly different process - one possibility being a pure deflagration explosion [80, 97].

Even though these very peculiar objects are classified as Type Ia SNe they do not obey traditional calibration relations and should be removed from any cosmological fits, if not they could contaminate results. So far we believe that all of these "truly peculiar" objects can be easily identified and removed from samples. In the right panel of Figure 3.4 we show examples of spectra from peculiar SNe.

In fact, also the "normal" SNe Ia show systematic variations that can be interpreted as subclasses. Examples of such normal subclassification are the Branch-types [16] and the high/low velocity gradient-types [10].

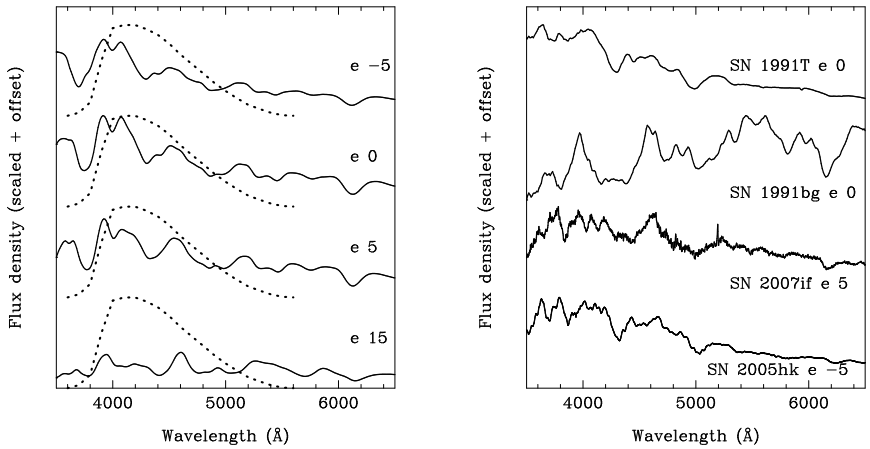

Figure 3.4: *Left panel:* Evolution of a normal Type Ia supernova with epoch (day with respect to light curve peak). The epoch is given for each template [templates from 64]. Dotted line shows the B-band filter transmission curve. *Right panel:* Peculiar Type Ia supernova subtypes. Included are SN 1991T and SN 1991bg templates at light curve peak [91], SN 2007if, a possible *Super-Chandrasekhar mass* SN, at epoch 5 [109] and SN 2005hk, a SN 2002cx-like SN, at epoch -5 [97]

3.3 How to Measure a Spectrum

During recent years the amount of available spectroscopic data of SNe Ia has rapidly increased. To obtain physical insight from these large samples, information needs to be quantified. One way to do so is through "spectral indicators", measurements of spectral properties.

As discussed above elements in the SN ejecta will absorb photons originally emitted by radioactive material in the inner layers, thus causing the typical pattern of "features" visible in SN Ia spectra. We will here introduce two spectral indicators measuring these features, pseudo-Equivalent Widths (pEWs) and line velocities.

In this analysis of spectral features we concentrate on seven regions, shown in Figure 3.5 for a typical spectrum at two different epochs. Each feature is labelled after the ion that normally dominates the absorption in this region (see Table 3.1), but most absorption lines are blends of several lines and should not be directly identified with physical properties. These regions will therefore sometimes just be identified as features 1 to 7.

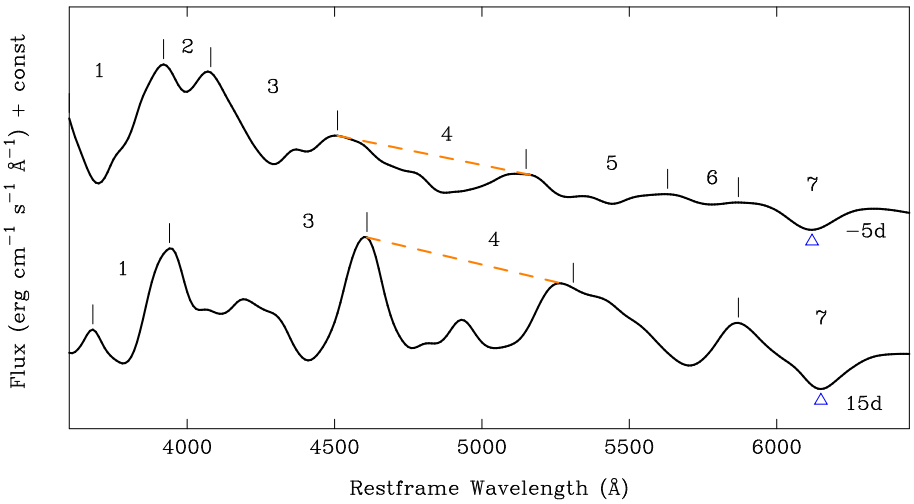

Figure 3.5: The feature regions used for the measurements of spectral indicators are shown for two template spectra at day −5 and 15 relative to light curve peak [templates from 64]. The *pseudo* continuum (dashed line) and line minimum (marked with triangle) are shown for two features (feature 4 and 7, respectively).

Spectral indicators are always measured on rest frame spectra.[12]

3.3.1 Pseudo-Equivalent Widths

For astrophysical objects with a well-defined continuum, the *Equivalent Width* (EW) of an absorption feature can be easily measured:

$$\mathrm{EW} = \sum_{i=1}^{N} \left(1 - \frac{f(\lambda_i)}{f_c(\lambda_i)}\right) \Delta\lambda_i, \tag{3.8}$$

where f is the observed flux and f_c is the continuum. The sum is taken over the wavelength region containing absorption. If, furthermore, the density structure is known and the absorption is caused by a single ion, this information can be used to deduce elemental abundances. For SNe Ia, the spectra are dominated by wide absorption features caused by mixed multiple absorption lines. The continuum can thus not be read directly from the observed data, and the physical interpretation of equivalent widths becomes

[12]See Chapter 8 for a definition of *rest frame*.

Table 3.1: Feature Boundaries and Minima

Feature	Dominating Line	Lower Region (Å)	Upper Region (Å)	Rest Wavelength (Å)
f1	Ca II H&K	3450 - 3800	3800 - 4100	3945.12
f2	Si II λ4000	3800 - 3950	4000 - 4200	4129.73
f3	Mg II λ4300	3850 - 4250	4300 - 4700	4481.20
f4	Fe II λ4800	4300 - 4700	4950 - 5600	5083.42
f5	S II W	5050 - 5300	5500 - 5750	5536.24
f6	Si II λ5800	5400 - 5700	5800 - 6000	6007.70
f7	Si II λ6150	5800 - 6100	6200 - 6600	6355.21

non-trivial. Nevertheless, we can measure equivalent widths if an unambiguous (pseudo) continuum can be *defined*. We do this following Folatelli [36] and Garavini et al. [43]. Lower and upper limits for the continuum is found at the wavelength positions of peak-flux within the lower and upper wavelength *regions*, respectively. These regions are given in Table 3.1. The pseudo-continuum is defined as the straight line between the flux of these lower and upper limits, with the choice of peaks optimised so that the pseudo continuum is maximised while not intersecting the spectrum.

With this pseudo-continuum a pseudo-Equivalent Width (pEW) can be calculated (as for EWs):

$$\mathrm{pEW} = \sum_{i=1}^{N} \left(1 - \frac{f(\lambda_i)}{f_c(\lambda_i)}\right) \Delta\lambda_i, \tag{3.9}$$

where f is the observed flux and f_c is the pseudo-continuum. The sum is now taken over all wavelength bins contained between the lower and upper limit.

The pEW definition has the advantage of not having to fit any function to the data (most features are clearly non-Gaussian) as well as being insensitive to multiplicative scaling between spectra.[13]

The *statistical* error is given by

$$\sigma^2_{\mathrm{pEW}} = \sum_{i=1}^{N} \left(\frac{\sigma_f^2(\lambda_i)}{f_c^2(\lambda_i)} + \frac{f^2(\lambda_i)}{f_c^4(\lambda_i)}\sigma^2_{f_c}(\lambda_i)\right) \Delta\lambda_i^2. \tag{3.10}$$

It consists of two parts, the first is obtained from the flux uncertainty of the observed spectrum, σ_f, while the second propagates the uncertainty from

[13]Note that pEWs are not insensitive to additive flux differences.

the choice of pseudo-continuum, σ_{f_c}.

3.3.2 Line Velocities

The position of absorption and emission features can also be used to probe SN properties. We study the wavelength minima of the features defined above. These are converted into velocities through the relativistic Doppler formula,

$$v_{\rm abs} = c\,\frac{(\lambda_m/\lambda_0)^2 - 1}{(\lambda_m/\lambda_0)^2 + 1}, \tag{3.11}$$

where λ_0 is the laboratory wavelength of the ions creating the feature and λ_m is the measured minima wavelength in the rest frame of the host galaxy. As λ_0 we use the *rest* wavelength of the ion that each feature was named after, these are given in Table 3.1 (5th column).

Measurements of $v_{\rm abs}$ yield information regarding the explosion kinematics as opposed to pEWs that are mainly affected by temperature. As for pEWs, it is often difficult to give a simple physical interpretation of line velocities for SNe Ia since most spectral features consist of blends of ions. Also, different ions dominate features at different epochs and thus shift the minimum position. SiII λ6150 (f7), typical of SNe Ia, most often yield unambiguous measurements and is thus usually the best estimate of the expansion velocity [although not always the most accurate, see e.g. 94].

3.3.3 Measurement Uncertainties

In addition to the statistical error, there are several sources of systematic uncertainties affecting spectral indicators. The two most serious are host contamination and noise differences:

- Light from the host galaxy in the spectrum can both change the shape of the feature and induce an additive flux change. Since host contamination varies with host galaxy types, and redshift, this can create systematic errors.
- Filtering or smoothing is necessary in order to identify the end points of spectral features. Over or under filtering can introduce a measurement bias.

These will be further discussed in Chapter 5.

Chapter 4

Supernova Cosmology and Systematic Errors

This chapter shows how the homogeneous SNe Ia introduced in Chapter 3 can be used to probe the cosmological parameters described in Chapter 2. The `SMOCK` framework (Paper A) is presented as a method to study how systematic uncertainties complicate this process. For further details regarding SNe Ia and cosmology, see e.g. Goobar and Leibundgut [46].

4.1 Light Curve Fitters

As discussed in Chapter 3, SNe Ia can be standardised using light curve properties. An algorithm doing so is called a *light curve fitter*. A number of such codes exist, e.g. SALT[49], SALT2[48], MLCS2k2[65], SiFTO[26] and SNooPy[21]. These all estimate light curve shape and colour, according to some parametrisation, and use these to correct peak luminosity.

For example, *SALT/SALT2* estimates the light curve width/shape as the *stretch*/x_1 parameter and a colour, c, describing reddening according to an empirically determined extinction law. MLCS2k2 output, on the other hand, consists of a light curve shape-dependent parameter Δ and the V-band extinction, A_V. The A_V parametrisation assumes that any reddening not corrected for by the Δ parameter can be described by a Milky Way-like extinction law. A further difference between these fitters concerns the *training samples*: MLCS2k2 only uses well measured nearby SNe to determine correction coefficients, while SALT(2) also includes high redshift data and makes a global empirical fit to all parameters.

Unfortunately these methods do not always yield compatible corrected

peak luminosities! The differences are most likely related to two of the large unknowns in current SN cosmology: the nature of reddening and possible low/high redshift differences (evolution?). The uncertain SN Ia UV-flux, hard to study in the local universe but observed at high redshifts, contributes to the latter effect [71]. These problems will be addressed below as systematic uncertainties.

4.2 The Hubble Diagram

The luminosity distance, d_L, as defined in Equation 2.11, contains information about cosmological parameters. For every theoretical model we can calculate the luminosity distance as a function of redshift. This is where Type Ia supernovae get useful: We can measure both redshifts (from the host galaxy emission lines) and, since they are standard candles, comparisons between different SNe yield the change in luminosity distance between the redshifts. These two distance estimates (luminosity distance vs. redshift) can thus be used to rule out cosmological models.[1]

Observed luminosities are usually written as logarithmic magnitudes m.[2] These are related to d_L through:

$$m(z) = M + 5 \log d_L + 25 \tag{4.1}$$

where M is the absolute (distance independent) magnitude and $m(z)$ the magnitude observed for an object at redshift z. For cosmological purposes the absolute magnitude M can be treated as a nuisance parameter since it is the relative brightness of Type Ia SNe that is compared. The parameter of interest is thus the *distance modulus* $\mu(z) = m(z) - M$. These magnitude redshift comparisons are usually called *Hubble diagrams*, in Figure 4.1 an example is shown.

What is actually restricted by Type Ia SNe is a linear combination of Ω_M and Ω_Λ ($0.8\Omega_M - 0.6\Omega_\Lambda \approx -0.2$). To provide further constraints, results are usually combined with other cosmological probes. Studies of the Cosmic Microwave Background or Baryon Acoustic Oscillations yield very different degeneracies compared with SNe. These results all confirm the cosmological

[1] That the relationship between the two different distance estimates, redshift and luminosity distance, contains new information can be (roughly) understood as follows: Redshift is caused by the "stretching" of photons due to expansion, while luminosity distance also contains information about the "area" of a sphere around the lightsource.

[2] See Chapter 8 for a definition of *magnitude*.

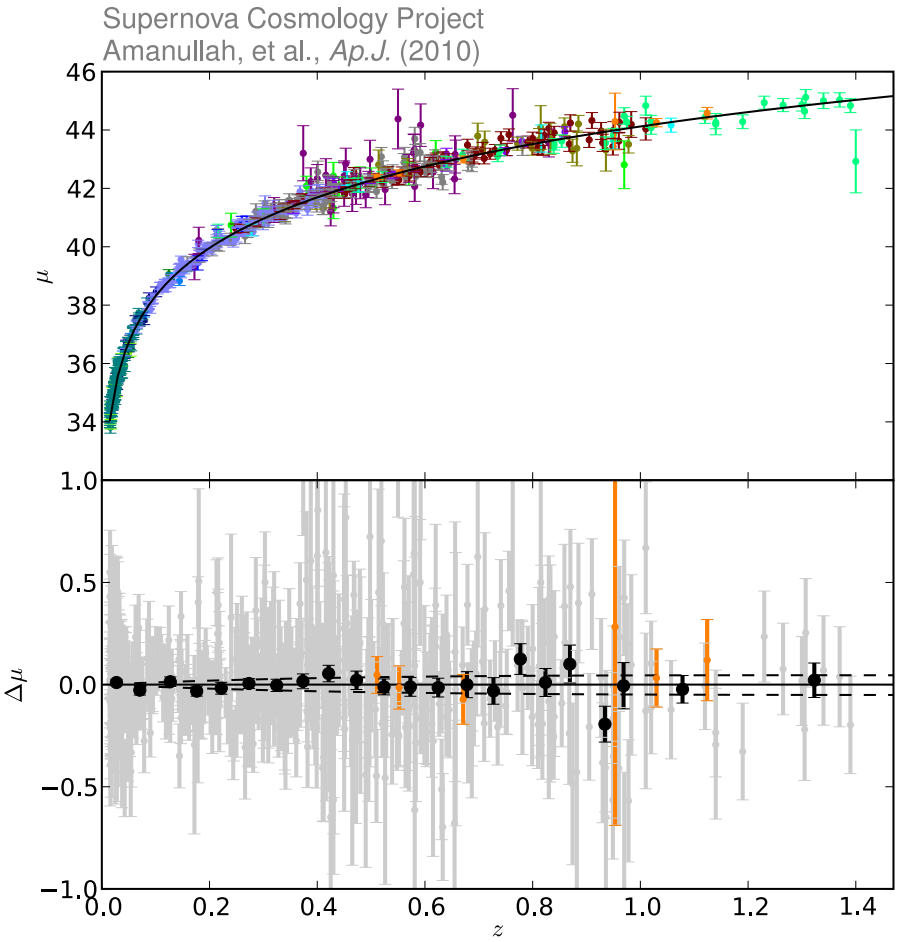

Figure 4.1: Hubble diagram based on the *Union2* sample from Amanullah et al. [2]. On the y-axis of the top panel is the distance modulus (magnitude after light curve and colour corrections, see Section 4.3.1), where the line corresponds to the best fit cosmology. If this best fit is subtracted we get the Hubble diagram residuals shown in the lower panel (bold points show binned averages). The x-axis show SN redshifts.

"standard model", $(\Omega_M, \Omega_\Lambda) = (0.27, 0.73)$. However, SNe by themselves are sufficient to rule out a matter dominated universe [74].

4.2.1 Supernova Surveys

Modern supernova cosmology demands high quality light curves, accurate typing and large volume (to ensure large statistics). This is achieved through large scale surveys where telescopes observe the same field every few days (a *cadence* of a few days) for an extended period of time. Each field is observed in a range of filters and these observations are compared with reference images. If any new object appears, this *could* be a Type Ia SN. Many candidates can be rejected when comparing magnitudes in the different filters (other transients have very different colours). Most, but not all, of the remaining objects are Type Ia SNe. To remove the last contaminating objects, optical spectra are obtained. Current surveys thus combine both frequent photometry (to obtain a light curve) and spectroscopy (to do final typing of all objects and get accurate redshifts).

4.3 Systematic Errors and SMOCK

During the years since the first methods to standardise Type Ia SNe were introduced the complications involved in supernova cosmology have been extensively studied. A range of possible uncertainties need to be taken into account. These uncertainties are what makes cosmology difficult - without them a handful SNe would be enough to determine the dark energy equation of state.

This section concerns these complications. The first part consists of a list of expected, possible or feared uncertainties. This list is not ordered and not complete, each item is only discussed very briefly and many items are highly correlated. It is mainly given in order to give a sense of the nature of possible uncertainties and motivate the second part of this chapter.

Systematic uncertainties dominate over statistical for current large data sets [5, 56, 71, 74, 125]. At the same time such uncertainties are usually non-linear, non-Gaussian and display complex correlations, and are thus not straightforward to include in fits of cosmological parameters. In section 4.3.2 we describe a Monte Carlo simulation framework, SMOCK, designed as a tool to quantify these uncertainties in a realistic way.

4.3.1 Some Examples of Systematic and Statistical Uncertainties

We will here shortly describe some possible systematic errors.

- *Calibration*
  Already for current SN cosmology surveys the calibration of the photometric observations is the dominating systematic uncertainty [25]. Counts registered on a unique CCD at a specific telescope, using a local filter, during one night, need to be converted into calibrated flux levels in a universal magnitude system (e.g. Vega). This conversion is not trivial. For example, filter transmission curves can change with time and thus subtly modify observed fluxes.

- *Colour*
  As discussed in Section 3.2.1 some SNe are redder than others. We know one source of reddening, absorption by dust in the Milky Way. This effect is well studied and using dust maps observations can be corrected [22, 111]. But reddening remains even after this correction. Current light curve fitters try to compensate for this, typically either explicitly assume reddening to be caused by host galaxy dust absorption (MLCS) or that it can be empirically determined as one wavelength-dependant extinction function (SALT2). If these methods fail, if for example reddening is caused by more than one process, we will bias cosmology. We will return to discuss reddening in Section 6.7.

- *Metallicity*
  Type Ia SN progenitors are usually described as C+O WDs, meaning that they originally consisted of H and He that subsequently burned to C and O. But as the universe ages, more metals are created (in supernovae!), and eventually a small fraction of metals will be mixed with the H and He forming the new star.[3] These metals are not destroyed and thus still exist in the exploding WD. Models indicate that even low levels of metals could have detectable effects on explosion properties, especially at bluer wavelengths [58, 79]. If such an effect exists it would increase with the total fraction of metals and thus with time, meaning it would affect distant (old) SNe differently than nearby (young). It is, however, not certain that an effect exists: metals could be concentrated in the centre of the WD and have negligible impact on the outer regions that are observed by us [19]. Konishi

[3] All elements heavier than Helium are considered metals.

et al. [73] reports a correlation between SN properties and metallicity measurements at the position of the SN.

- *Asphericity*
  Are Type Ia SNe completely spherical? There are both theoretical arguments (SNe have a companion), models (showing clumps in the ejecta) and observations (e.g. polarisation levels) telling us that this is not the case [69, 123]. Maeda et al. [84] show that SNe exhibit systematically different nebular line velocity shifts and provide a simple asymmetric model to explain these. Does the SN brightness then vary with viewing angle?

- *Progenitor*
  It is currently accepted that a Type Ia SN is caused by thermonuclear runaway of a C+O WD. But many unknowns remain: Which is the real explosion scenario, or do both the single and double degenerate channel exist? Are there limits on allowed progenitor metallicity? What sort of mass-transfer is needed? How nearby and massive must the companion be? Are there limits on rotation? No Type Ia system has so far been observed before explosion. For one case, that of Tycho Brahes SN 1572, there are claims that the companion has been detected [106].

- *K-correction*
  When constructing a Hubble Diagram the peak luminosity in the *rest*-frame B band is usually used, and the difference between *rest*-frame B and *rest*-frame V magnitudes are used to determine the colour. However, when observing SNe we do so in the *observer*-frame. All magnitudes we obtain are thus in filters redshifted with respect to the ones we would like to use when doing cosmology. These filter discrepancies are known and can, in principle, be corrected for. Corrections that convert observed magnitudes to rest frame magnitudes are called K-corrections [72]. However, a *perfect* correction demands that both correct filter functions are used and that the supernova spectrum at the epoch of observation is known, which is not realistically achievable. In practice a more or less suitable template spectrum is used [64].

- *Host galaxies*
  Type Ia SNe occur in all types of galaxies, but show systematic variations. It is well documented that star forming, late type galaxies host brighter SNe with wider light curve shape [52]. Further, the rate of SNe vary, possibly explained by two populations, one with the SN

rate proportional to star formation rate ("prompt") and one with the rate proportional to mass ("delayed"), with slightly different average parameters [61, 110]. Recently, luminosity variations not captured by light curve properties have been reported in host galaxy studies [70, 78, 114]. Section 6.6 discusses relations between host galaxy and spectroscopic properties.

- *Evolution with redshift*
  Many of the effects discussed here (like metallicity/host galaxy differences) could imply some level of evolution: distant SNe having different properties than local. Since the standard candle method in principle relies on the candles not evolving, this *could* be problematic. It *is* not necessarily so since supernova cosmology only demands that we sample *all types* of SNe locally (and thus can verify their standardisation). If a non-corrected/non-detected evolution exists, however, this would directly bias cosmological results and exactly mimic a changing expansion rate of the universe. An example of an astrophysical effect causing such evolution is intergalactic "grey" dust [45], constant absorption for all wavelengths [although the cosmological uncertainty from such dust is now very constrained, see 93]. Evolution of *spectroscopic properties* will be discussed in Section 6.4.

- *Redshift uncertainties*
  Current supernova surveys obtain accurate redshifts from spectra either of the host or (slightly less accurate) of the supernova. Future huge volume photometric only surveys like the Dark Energy Survey (DES) or the Large Synoptic Survey Telescope (LSST) will not be able to provide such spectra, instead redshifts will be estimated using photometry. This introduces fundamental uncertainties and it is not certain that large statistics will compensate [29].

- *Non-normal or misidentified SNe Ia*
  The non-normal SNe Ia subtypes shown in Figure 3.4 all have different peak luminosities. Some can be standardised in the normal procedure (and thus used for cosmology), others not. There are also other transients (Core-Collapse SNe, AGNs) that could be mistaken for SNe Ia and thus bias cosmology. Currently, misidentified SNe Ia are avoided using combined photometric and spectroscopic data.[4] Once

[4] Even spectroscopic identification is sometimes very hard, especially in the presence of noise. Type Ib/c SNe, for example, can look very much like SNe Ia where no silicon is seen (which can happen roughly one week after max) [82].

more, future photometric-only surveys will have to demonstrate that such objects do not bias the results.

- *Gravitational lensing*
  All distant light sources can be affected by gravitational lensing. This is wavelength independent and thus not detectable through changes in spectra. The average magnification is zero but with an asymmetrical distribution; most SNe experience very small demagnification while some rare events are highly magnified [11, 66].

- *Malmquist bias*
  If surveys are not limited by volume but by brightness, only the brightest objects are observed at the farthest distances. This could bias results if objects at all distances are assumed to have the same average properties.

- *Homogeneity-isotropy*
  The ΛCDM framework assumes that the universe is homogeneous and isotropic, and that the small scale clumps and voids we see can be averaged out. Supernova data now puts very stringent constraints on fully inhomogeneous models [13], but it is still unclear whether averaging of the matter density can modify the cosmological parameters when evaluated in the ΛCDM framework.

4.3.2 SMOCK: Quantifying SN Systematic Errors Through MC Studies

Systematic errors do not in general follow a simple parametric form that can be added to error estimates. They are often non-linear and non-Gaussian. Systematic errors cause measurements to be highly correlated in a non-predictable way. It is thus far from clear how the above uncertainties propagate to cosmological parameter estimations. Current SN samples are dominated by systematic errors [56, 74]. To make measurements more precise these systematic errors need to be first understood and then limited. As a first step we need to quantify their effect on cosmological parameter estimation.

In Paper A, the Supernova MOCK (SMOCK) code is presented. This is a flexible Monte Carlo simulation framework designed to incorporate any combination of arbitrarily shaped or correlated uncertainties. Through this method no assumptions regarding the errors need to be made, as would be

the case for e.g. Fisher Matrix analysis.[5] The drawback with any simulation is the required computational time.

The SMOCK structure

The simulation follows a simple loop. As input a given distribution of data parameters are used (like redshift, magnitudes and light curve properties). The distributions can either be taken from an observed data set or from simulated data.

Simulations then proceed using a given set of run parameters. These parameters determine exactly which systematic uncertainty models that should be tested on the data set. Any given model affecting any of the data parameters can be included, provided probability distributions exist. We then repeat the following steps:

1. Every data point is shifted. This includes randomising all parameters given model probability distributions. All such changes are then propagated to each individual redshift, magnitude and error. Statistical uncertainty, like measurement errors and intrinsic dispersion, are also included.

2. Using the shifted data points, a cosmological fit is performed. The best-fit cosmology is saved.

This process is continued until convergence.[6] After run completion statistical tests can be made on the set of best-fit cosmologies obtained. In this way both the most-likely fit and e.g. the 68% confidence regions can be calculated. If only statistical errors are included the method yields contours corresponding to a "normal" fit to the data.

The final analysis step is then to compare results from different runs in order to estimate the effects of the added systematic uncertainties on cosmological parameters. When different runs with increasing systematic *model* uncertainties are performed the increased *cosmological* fit uncertainties are obtained as functions of the model uncertainties.

Some examples of implemented uncertainties:

- Evolution with redshift.

[5] Realistic Fisher Matrix studies can be made, *provided correct correlation matrices exist*. Another possible use for SMOCK is to construct such matrices.

[6] This is assumed to be when additional runs do not change the distribution of best-fit cosmologies.

- Dust effects through variations in R_V, possibly with redshift.
- Typical gravitational lensing errors as calculated in SNOC [47].
- Malmquist bias through removing faint objects in different redshift bins (after adding intrinsic dispersion).
- Light curve fitter output differences.
- Metallicity effects [using the parametrisation of 100].

For a complete discussion see Paper A. The framework was designed to allow for easy incorporation of new sources of uncertainty as they are encountered.

4.3.3 SMOCK Systematic Error Estimations

A long range of different combinations of uncertainties were applied to different data samples: (i) the *Gold* data set [104] (ii) the SDSS dataset [71] and (iii) the proposed SNAP distribution ($\sim$ 2000 SNe distributed up to $z = 1.7$).

The results are most easily accessible through the simple graphical interface.[7] Here the magnitude of different uncertainties can can be quickly compared. See Figure 4.2 for a sample screenshot. The general conclusions from SMOCK runs based on current data are that uncertainties related to reddening and evolution are the dominating astrophysical systematic uncertainties.

Survey optimisation: SNAP

The SMOCK code was originally developed as part of analysis work during the planning stage of the SNAP satellite.[8] The main target of this mission was to remove/reduce all systematic uncertainties that affect supernova cosmology. To do this all parameters should be explored and optimised so that uncertainties are minimised. Examples of such parameters include: Filter shape, exposure times (in different filters) and SN redshift distribution. These parameters can be studied as different models of systematic errors are applied. SMOCK provides a way to test how to choose these in order to minimise uncertainties.

[7] Accessible at http://www.physto.se/~nordin/smock/
[8] See snap.lbl.gov

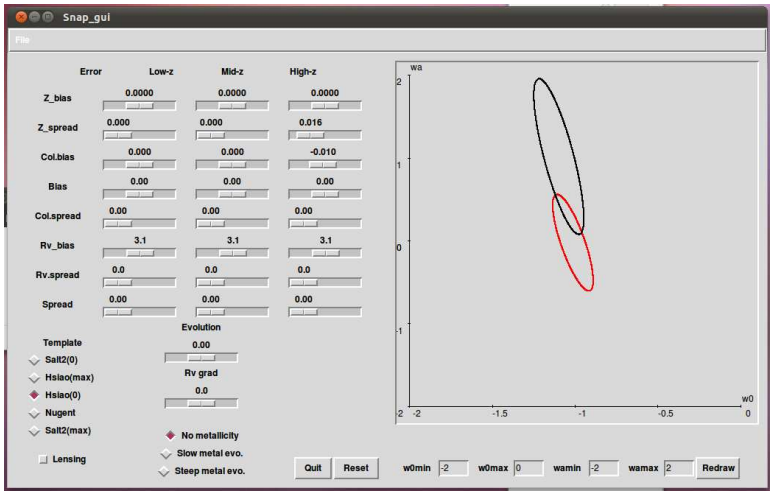

Figure 4.2: Screenshot of the graphical interface collecting SMOCK studies of systematic errors in a SNAP sized sample.

Chapter 5

The SDSS NTT/NOT Spectroscopic Sample

In this Chapter, the SDSS NTT/NOT spectroscopic sample is introduced. This includes a discussion regarding host galaxy contamination estimation and noise filtering.

5.1 The Sloan Digital Sky Survey II Supernova Survey

The Sloan Digital Sky Survey (SDSS) has performed a number of high quality astronomical surveys since 2000.[1] The dedicated 2.5-meter telescope at Apache Point Observatory, New Mexico, together with an automated reduction pipeline, has allowed deep and repeated surveys of large fractions of the sky.

The SDSS Supernova Survey (SDSS-SN) operated as part of the second SDSS run (2005-2008). SDSS-SN was specifically designed to detect and provide high quality multi-band light curves of supernovae in the previously rarely observed intermediate redshift range $0.1 - 0.4$. During three 3-month campaigns a 300 square degree field was observed with a target cadence of a few days. All observations were made using five optical filters: u,g,r,i,z. See Frieman et al. [40] for a description of the survey strategy and Holtzman et al. [60] for a description of the photometric pipeline. The SDSS redshift range allows a sharp transition between the expansion rate locally and in the distant universe to be ruled out. The first year cosmological results are

[1] The SDSS Web Site is `http://www.sdss.org/`.

described in Kessler et al. [71]. Alternative dark energy models are examined in Sollerman et al. [113] and a redshift limited study performed in Lampeitl et al. [77].

An essential requirement for the use of SDSS supernovae for cosmology is that they are correctly typed as Type Ia supernovae. Since other transient phenomena have different luminosities they will bias cosmological parameter *if assumed to be SNe Ia*. To avoid such misclassifications a spectroscopic follow-up campaign was initiated at a number of telescopes. All promising supernova candidates identified in the photometric pipeline and verified using manual scanning were sent to a queue for spectroscopic confirmation. Participating facilities would then observe candidates from this list. The candidate selection algorithm is described in Sako et al. [107] and the first year spectroscopic observations in Zheng et al. [128].

Two of the most heavily involved telescopes were the Nordic Optical Telescope (NOT), at the Observatorio del Roque de los Muchachos on La Palma, Spain, and the New Technology Telescope (NTT) at the La Silla Observatory, Chile. During the 2006 and 2007 campaigns in total 45 nights were awarded at the NOT and the NTT, out of which 41 had sufficiently good weather for observations. The thus obtained spectra constitute the *SDSS NTT/NOT* sample. This is described in full detail in Paper B.

5.2 Observations, Data Reduction and Typing

During 32 nights with good conditions 244 spectra of SN candidates were obtained at the NTT telescope. The NTT has a 3.58-m primary mirror and observations were made using the ESO Multi-Mode Instrument (EMMI; Dekker et al. [30]). The final wavelength coverage is 3800 to 9200 Å, the wavelength dispersion (resolution) 1.74 Å per pixel, and the spatial resolution $0\farcs166$ per pixel before binning. A binning of 2x2 was used.[2]

The NOT has a 2.56-m mirror and spectra were obtained using the Andalucia Faint Object Spectrograph and Camera (ALFOSC). NOT spectra have a wavelength range from 3200 to 9100 Å, a wavelength dispersion of 3.0 Å per pixel, and a spatial resolution of $0\farcs19$ per pixel. During 9 nights with good observing conditions 46 spectra of target SNe were obtained.[3]

Exposure times were typically 1800 seconds, but could vary between 300

[2]The NTT observations were acquired in the ESO programmes 077.A-0437, 078.A-0325, 079.A-0715 and 080.A-0024 under PI Robert Nichol.

[3]The NOT observations were acquired in the programmes with proposal numbers 34-004, 35-023 and 36-010 under PI Maximilian Stritzinger.

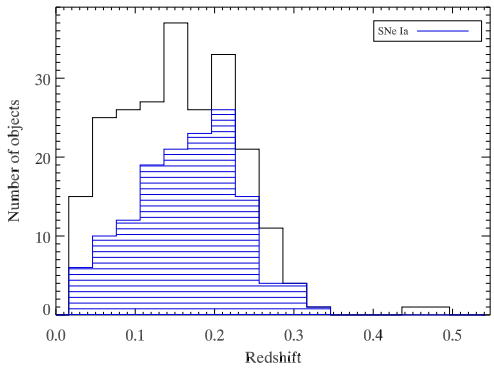

Figure 5.1: Redshift distribution of the 228 observed objects at the NTT and the NOT with a known redshift. The subset of objects classified as SNe Ia is shown in the striped histogram. Figure from Paper B.

and 3600 seconds depending on target luminosity and observing conditions. Each unique object was assigned an SDSS ID (see Paper B for corresponding IAU ID's). Out of the 238 targets, 84 had prior galaxy redshifts from SDSS DR7, 102 objects had the redshift determined from galaxy lines, 40 from SN features and two from (rough) template fits. Some of these redshifts were determined from NTT/NOT spectra, but also observations from other telescopes were used. For 10 objects, no redshift could be determined. In Figure 5.1 we show the redshift distribution for all targets with redshift.

A spectroscopic reduction pipeline was constructed using a combination of `IRAF`[4] routines and our own software. Reduction was mainly standard *Bias subtraction*, *Flat fielding*, *Spectral extraction*, *Wavelength and flux calibration*, *Telluric removal* and *Correction for Milky-Way dust extinction*.[5]

The slit admitting light into the spectrograph was often not aligned with the *parallactic angle*.[6] Instead it was usually oriented so as to pass both through the SN and through the core of the host galaxy, or to avoid bright objects in the field. The observations will thus suffer from *differential atmospheric refraction* (DAR), a kind of *slit loss*, in practice wavelength

[4] `IRAF` is distributed by the National Optical Astronomy Observatories, which are operated by the Association of Universities for Research in Astronomy, Inc., under cooperative agreement with the National Science Foundation.

[5] See Chapter 8 for a definition of *reduction*.

[6] See Chapter 8 for a definition of *parallactic angle*.

Table 5.1: Number of Spectra and Unique Objects.

	Spectra	Objects
Total	290	238
with redshift	280	228
SN Ia	169	141
with good light curve	127	108
SN Ia?	3	3
SN II	26	23
SN Ib/c	12	8
Not SN	19	16
Galaxy	14	12
Unclassified	61	47

dependant flux loss.[7] Furthermore, the SDSS-SN field positions on the sky forced observations at high airmasses (closer to the horizon), increasing the DAR magnitude. Several spectra are thus severely distorted by this effect, which has implications e.g. for the removal of host galaxy contamination (see below). DAR was estimated for each observation, see Section 5 in Paper B for details.

Finally, the type of astrophysical source of each observed spectrum was identified through a combination of manual inspection and use of the template fitting software SNID [SuperNova IDentification; 15]. After these steps we find that the SN Ia sample contains 169 spectra of 141 individual SNe, plus 3 likely SNe Ia. In addition, we also obtained 26 spectra of 23 SNe II and 12 spectra of 8 SNe Ib/c. The number of spectra and the number of unique objects are summarised in Table 5.1. Several likely non-normal SNe Ia were found. For example, SN 2007ie (SDSS 17176), show strong indications of being a SN 2002cx-like SN. If allowing the redshift to vary freely, different supernova templates could match, although SN 2002cx yields the best match. If we fix the redshift to the SDSS DR7 redshift SNID provides a clear SN 2002cx identification. In Figure 5.2, some of the SNID fits to SN 2007ie are shown. We thus see that also the very subluminous SN 2002cx-like SNe are detected at higher redshifts, and need to be accounted for in photometric surveys.

[7] See Chapter 8 for a definition of *DAR, slit loss.*

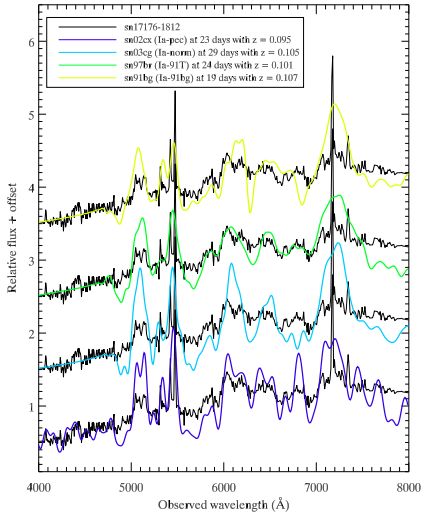

Figure 5.2: The observed spectrum of SDSS ID 17176 (SN 2007ie) together with (thin) lines showing different typical spectra of SN subtypes (see legend). Figure from Paper B.

5.3 Host Galaxy SED Estimation

A SN spectrum will contain a superposition of supernova light and light from the host galaxy. For nearby SNe the size of the galaxy is large compared with the supernova Point Spread Function (PSF), allowing galaxy light to be efficiently removed in the spectral reduction process. For more distant objects this is not possible, and at some distance both host galaxy and supernova will appear as superposed point sources.

The NTT/NOT SNe, at intermediate redshifts, display varying degrees of host contamination. For accurate studies of spectral indicators, like pseudo-Equivalent Widths, such contamination needs to be removed. This Section describes the host-galaxy subtraction method used and Monte-Carlo tests of its success. This method is specifically tailored to allow measurements of pEWs and line velocities, and might not be suitable for other applications (e.g. flux ratio measurements and computer modelling). Only SNe Ia spectra were host subtracted.

5.3.1 Host Galaxy Subtraction Introduction

In the past, several different techniques have been used to subtract the host-galaxy contribution from observed spectra. If a separate spectrum of the host galaxy exists this can be subtracted [the contamination level is either fitted or estimated from photometry, see e.g. 32, 63]. For the vast majority of the NTT/NOT spectra, no good quality spectra of the host galaxy at the location of the SN was accessible at the time of this work and using a real galaxy spectrum was thus excluded. There are also host-galaxy subtraction methods which separate the two components, SN och galaxy, directly in the two dimensional spectrogram [9]. However, this requires higher resolution of the data than that of the NTT/NOT data set.

Instead *galaxy eigenspectra*, determined from Principal Component Analysis (PCA) of typical galaxy spectra [127] were used to model the host galaxy. Similar methods were used by Zheng et al. [128] and Foley et al. [38]. For a large fraction of the moderately contaminated spectra (10-60% contamination, estimated from photometry, in the g-band) we found this subtraction method to yield good results.[8]

DAR/slit-loss creates additional difficulties for the host-galaxy subtraction since the supernova (being a point source) is affected differently than its host galaxy (being an extended source). Furthermore, galaxies look more and more like point sources at higher redshifts. This has to be accounted for in the subtraction process.

5.3.2 Host Galaxy Subtraction Method

The spectral energy distribution (SED) of the host galaxy was estimated through minimising the difference between the observed spectrum and a combination of a SN template and a set of galaxy eigencomponent spectra. The SED fitted to the observed spectrum can be described with the formula

$$f_{\rm fit}(\lambda) = a_0 s(\lambda) \cdot f_{\rm SN}(\lambda) + \sum_{i=1}^{n} a_i g_i(\lambda), \tag{5.1}$$

where $f_{\rm SN}(\lambda)$ is the SN template, $g_i(\lambda)$ the galaxy eigencomponent spectra, $s(\lambda)$ is a second degree polynomial and a_i weights which are fitted in the subtraction.

[8] Some part of the host-galaxy light, at least for host galaxies with larger spatial extent on the CCD, were removed during a linear background fit in the reduction of the 2d-spectra. For these spectra the host-galaxy contamination that was fitted was thus the *residual* from the reduction.

The galaxy eigencomponent spectra were created in a PCA analysis of 170 000 SDSS galaxy spectra [127]. The three most dominant eigenspectra have been shown to describe 99% of all galaxies.[9] In the fit we included the constraint that the total galaxy flux must be positive.

For the SN template we use templates published by Hsiao et al. [64] and in each fit we tried all templates with epochs ±5 days from the epoch of the spectrum. We also included templates of more peculiar SNe, SN 1991bg and SN 1991T [91], to compare with non-normal SNe. None of our spectra were well fitted with the SN 1991bg template (not surprising since there will be a bias against such objects due to their faintness). Some spectra had marginally better fits with a SN 1991T template, but for these the template used did not significantly affect the subtracted SN spectrum.

The second degree polynomial, $s(\lambda)$, multiplied with the SN template was introduced to account for reddening (e.g. due to host galaxy dust extinction) and DAR/slit-loss effects. During observations, the object was centred on the slit in the red part of the spectrum, and thus differential slit losses due to atmospheric refraction, when present, predominantly affects the blue end (as does extinction). The second degree polynomial was fixed to have $s(\lambda_1) \equiv 1$ with $\lambda_1 = 6600$ Å and $s(\lambda) < 1$ for all other wavelengths. The value of λ_1 was chosen to correspond to the effective wavelength where most spectra were centred on the slit. DAR is in general not symmetric around the centering wavelength, but since the fit during host-galaxy subtraction was only made between 4000 Å and 6000 Å, the behaviour of the slit loss function at longer wavelengths did not affect the fit. The polynomial is only multiplied with the SN template, and not with the galaxy. This was done since galaxies, not being point sources, are significantly less affected by slit loss.

Figure 5.3 shows examples of observed spectra together with the estimated host galaxy SED. Host contaminations in this Figure range from very high (77%) to very low but including reddening/slit loss. For moderate contamination, 10 to 60% galaxy light in the g-band, the multiplicative host-galaxy subtraction works well. *Within these limits the best fit galaxy SED is subtracted from the observed spectrum before any measurements are done.* For spectra with very low contamination no subtraction is done while spectra with very high contamination are excluded from further analysis.

[9] The fit can be made arbitrarily complex through the inclusion of more galaxy eigencomponent spectra (to the existing three), but this extension was not used in the final studies since the fits did not improve significantly while the computational demands increase drastically.

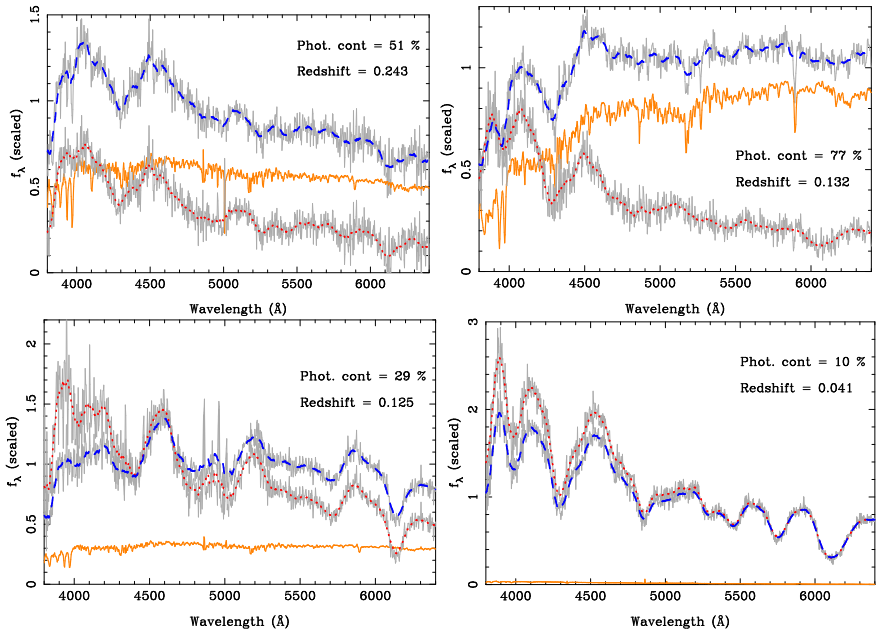

Figure 5.3: Display of sample host galaxy subtractions of SDSS SN16637, 12907, 17886 and 13894 (clockwise from top left, rest frame epochs -1, 0, -4 and 9 days). All flux values (y-axis) have been scaled. Wavelength (x-axis) is rest frame wavelength. Dashed blue lines show the unsubtracted and dotted red lines the final host galaxy subtracted *slit loss/reddening corrected* spectra and orange solid lines best fit galaxy SEDs. Grey lines show unsmoothed spectra. The galaxy contaminations estimated from photometry (g-band) and redshift have been written in each panel.

5.3.3 Alternative Subtraction Methods

Several modified versions of this host subtraction were tried: Other sets of eigencomponent spectra, more eigencomponent spectra, unrestricted polynomial $s(\lambda)$ and slit loss applied to the host galaxy. For individual spectra one of these alternative methods might achieve better fits, but globally they were all either less stable or as good but with significantly more parameters to fit.

Two methods relaxing the dependence on SN template were also implemented: Linear fits using all nearby SN spectra as SN templates and photometry fixed galaxy subtraction where the host galaxy photometry is used to constrain the galaxy shape and proportion. The first method incorporates a large amount of templates and the second does not use any

template at all. However, in general the multiplicative method including the slit loss/reddening correction was found to be superior in most cases and more stable for a sample with NTT/NOT specifications.

5.3.4 Evaluating the Subtraction Pipeline

To evaluate the subtraction methods, a large number of simulated "*fake*" spectra were constructed and run through the subtraction pipeline. Each *fake* spectrum was constructed through a combination of a SN and a galaxy spectrum, redshifted to some distance. Reddening and DAR were added to the SN spectrum and finally varying levels of random noise. All parameters (redshift, spectral epoch, host-galaxy contamination, reddening, differential slit loss and noise) were drawn from distributions that match the NTT/NOT data set. In constructing these fake spectra we avoided all templates/functions that were used in the host-galaxy subtraction pipeline (as this would make the fit trivial). See Paper B and Appendix A of Paper C for full details.

The simulations were evaluated using a range of different tests. For all fake spectra we compared the input SN and galaxy spectra with the SN and galaxy as estimated by the host-galaxy subtraction pipeline. In Figure 5.4 we show how the *difference* between input and estimated (output) contamination varies with input contamination (in the g band). Note that we get a more accurate estimation with higher contamination levels; it is hard to correctly find the galaxy SED with only a small galaxy light fraction.[10] For objects with very low contamination it can thus be advantageous not to subtract the estimated host galaxy light since the correction is smaller than the uncertainty in the correction.

We have also studied direct effects on spectral indicator measurements caused by the host subtraction pipeline. All of the created fake spectra were processed through the host subtraction pipeline and spectral indicators were measured. The measured spectral indicators could then be compared with the ones obtained from the original SN spectrum. The subtractions are thus evaluated with respect to how well correct indicators were measured. Sample simulation results are presented in Figure 5.5. In general simulations are stable with the following characteristics: A small bias for very low contamination levels that decreases with added contamination and a random dispersion that increases with contamination. The sizes of such effects vary slightly from feature to feature. For each feature, epoch and spectral

[10] Small levels of remaining host light in the SN templates used in the MC study would contribute to this effect.

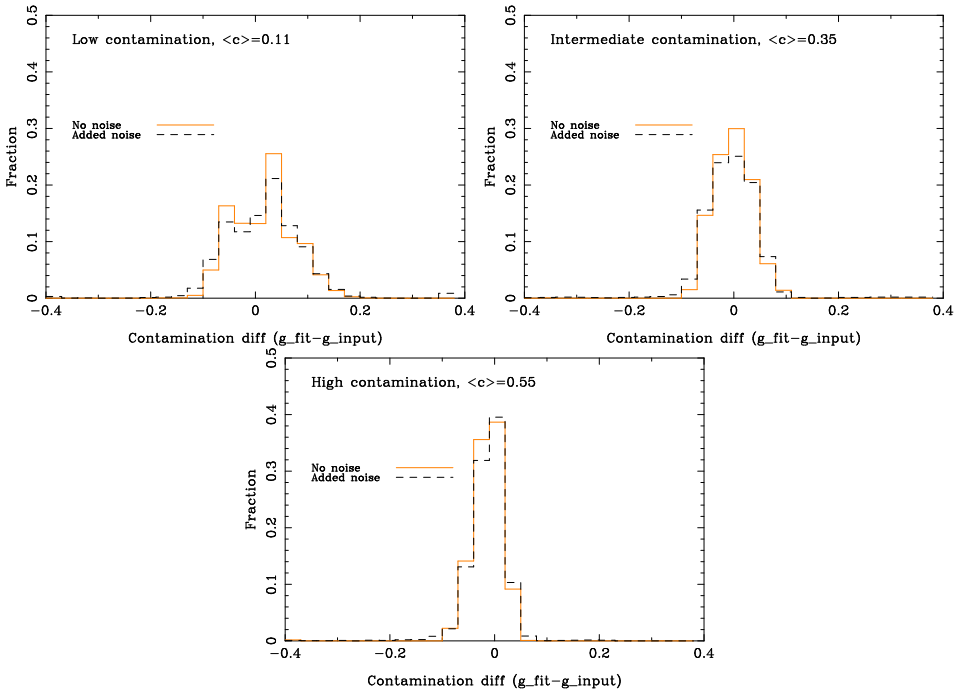

Figure 5.4: *Error in estimated contamination.* The difference between the g-band host-galaxy contamination that was introduced in the construction of fake spectra (g_input) and the contamination that was obtained during host-galaxy subtraction (g_fit) for three different bins in g_input. The mean contamination for each bin is given in the respective panel as $< c >$. The contamination was calculated as the percentage of the total flux in the observed SDSS g band which comes from the galaxy. The solid histogram corresponds to simulations without added noise while the dashed line corresponds to where noise is added. The dispersion is largest for small input contaminations. The number of outliers increase from 0.9% to 2% when noise is added.

indicator combination the systematic uncertainty and bias as functions of contamination are recorded and used as a *Host subtraction systematic error* in the spectral studies of Chapter 6.

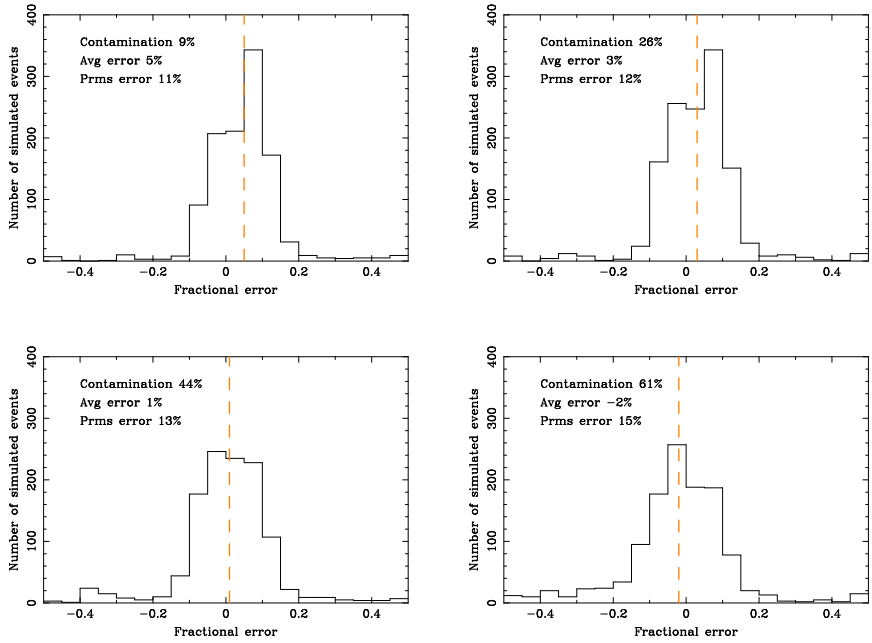

Figure 5.5: *Error in indicator measurements.* For every simulated spectrum the indicators measured on the host subtracted version are compared with the true non-host contaminated values. These plots are based on pEW f3; other indicators show similar results. The fractional error (true value subtracted from "fake" measurement, divided by true measurement) is used so that all templates of different epochs and subtypes can be added and errors analysed as functions of contamination. The panels show the distribution of errors, divided into four contamination bins ($0-17.5$,$17.5-35$,$35-52.5$ and $52.5-70\%$ in g band). The average contamination, average error and Population RMS is printed for each bin. The average error (dashed line) indicates a small bias, *decreasing* with contamination. The dispersion indicates a random error from host subtraction, increasing with contamination.

5.4 Filtering and Uncertainties Due to Noise

The level of random noise varies greatly in the NTT/NOT sample. The spectra were initially obtained mainly to provide the type of the transient,

and observations were optimised so that as many candidates as possible could be observed each night. Many SN spectra are thus noisy, making studies of spectral properties impossible unless some kind of noise filter is applied. For high signal-to-noise (S/N) SN spectra, the conventional solution is to apply a mild filter to remove the high-frequency noise. For noisy data, however, it is no longer obvious what filter strength to use or how accurate results are.

According to the definition, pseudo-Equivalent Widths run from the wavelength of one flux extremum point to another. This makes such measurements very sensitive to noise: if any noise peaks remain, the pseudo continuum will be defined from these points. To remove noise, and create unbiased data, strong filtering is needed for low signal-to-noise data. We would, however, not want to filter high S/N spectra (at any redshift) too much since this would destroy information. We would also like to estimate the combined noise and filter uncertainties.

A series of Monte Carlo simulations were run in order to (i) compare filter methods, (ii) determine filter parameters and (iii) estimate associated uncertainties. It was found that a simple boxcar filter (simply averaging over a wavelength range) works well provided the boxcar width is adjusted depending on noise level in the spectral range studied. A second set of MC simulations were run to determine the filter widths to use and the typical errors caused by noise for each each feature and epoch. These errors, as functions of noise level, are used as *Noise systematic error* in the spectral studies of Chapter 6. See Appendix B of Paper C for a full description of this process.

5.5 The Final Sample

The final SDSS NTT/NOT sample is described in detail in Paper B and the spectra are publicly available.[11] Figure 5.6 shows a sample of high signal-to-noise spectra and Figure 5.7 shows noisier more distant SNe.

[11] Can be obtained at `www.physto.se/~linda/spectra/nttnot.html`.

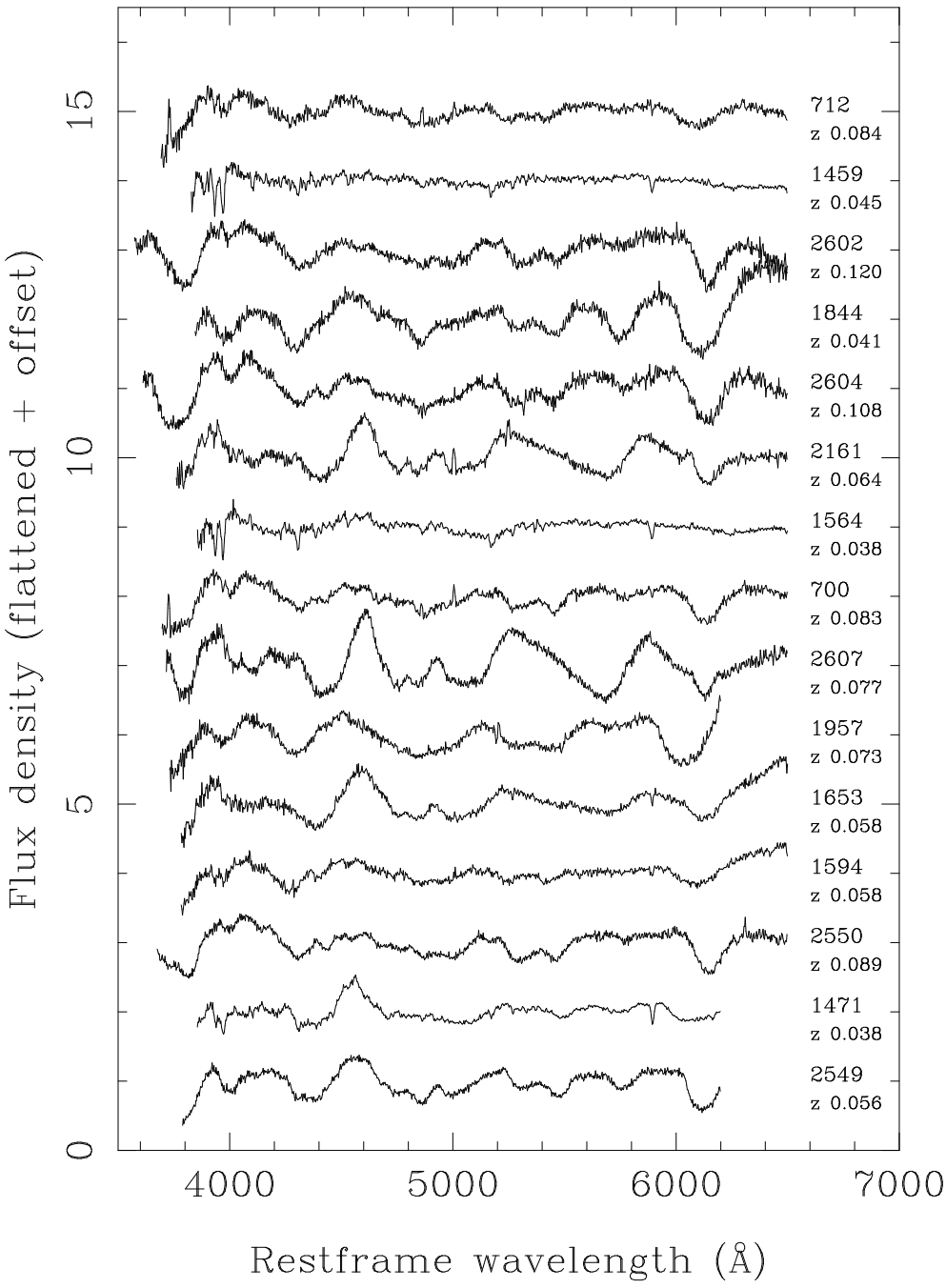

Figure 5.6: A sample of high signal-to-noise spectra from the NTT/NOT sample. After each spectrum we include the Spectrum ID (SPID) and redshift.

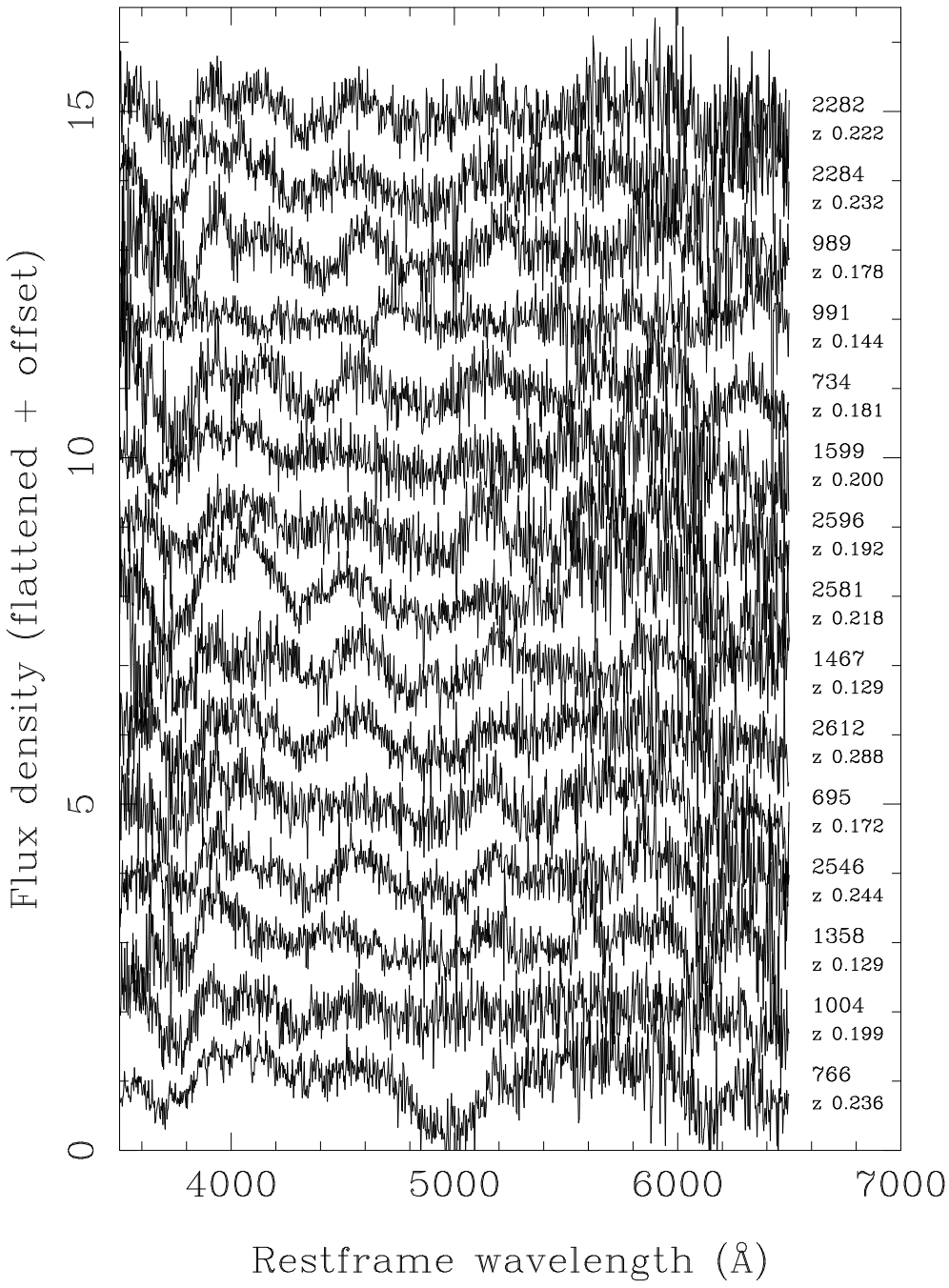

Figure 5.7: A sample of lower signal-to-noise (but usable) spectra from the NTT/NOT sample. After each spectrum we include the Spectrum ID (SPID) and redshift.

Chapter 6

Spectral Properties of SNe Ia up to z $\sim$ 0.3

Armed with the spectroscopic indicators defined in Chapter 3 and the intermediate redshift NTT/NOT sample introduced in Chapter 5 we can now make quantitative studies of SNe Ia spectroscopic properties. The goal is to investigate some of the uncertainties discussed in Chapter 4 and, if possible, sketch how sharper constraints on cosmological parameters could be achieved.

6.1 Introduction

The spectra of SNe Ia have long been used as a tool for understanding these phenomena. Studies have typically been qualitative examinations of individual nearby objects.

With the huge increase in the number of observed SNe during the last decade and the wish to do ever better SN cosmology, a number of quantitative studies of collections of spectra have been made during recent years. These use some combination of spectroscopic indicators: pseudo-Equivalent Widths (pEWs), line velocities or flux ratios. The two first types are described in Section 3.3, the latter consists in measuring the ratio of flux at specified wavelengths. Folatelli [36] and Garavini et al. [43] introduced pEWs and searched for evolution with redshift using Supernova Cosmology Project (SCP) data. Spectra from the SuperNova Legacy Survey (SNLS) are probed for evolution in Bronder et al. [20] [later continued in 122] and line velocity properties of the ESSENCE survey in Blondin et al. [14]. These studies were limited by the sample sizes and the noise in the high redshift

data.

The latter of these limitations can be targeted using *composite spectra*. An average high redshift spectrum is compared with the corresponding average low redshift spectrum. Using these methods both the ESSENCE [38] and SNLS [115] collaborations tentatively detect evolution towards shallower average spectroscopic features at higher redshifts. Composite spectra are, however, very sensitive to how they are made and which spectra are included. It is thus very hard to say what is causing a possible difference between two composite spectra.

The SDSS NTT/NOT spectra provide a key opportunity to study spectroscopic properties of SNe Ia. First, the SN population is drawn from an interesting redshift range, where evolution could be expected, yet the SNe are close enough to yield a reasonably high S/N in individual spectra (with 2.5 - 4 m class telescopes). Secondly, this data set is large enough to allow large scale statistical tests. Thirdly, high quality SDSS light curves exist for all SNe.

Spectroscopic indicators can be used to study the physics behind SNe Ia and possibly provide a sharper SN Ia standard candle. The width of the photometric light curve (powered by radiative decay) is clearly related to both the relative depth of silicon features ["Si-ratio", 92] and certain pEWs [20, 43]. Recently it has been suggested that both flux-ratios [6] and line velocities [124] can be used to standardise SNe Ia beyond what current light curve fitters do. However, hitherto suggested methods for this demand spectral quality very hard to achieve at cosmological redshifts. The SDSS NTT/NOT sample can be used to search for realistic ways to improve SN distance estimates.

6.2 Data Samples

We will here present the data used for quantitative studies of spectroscopic properties. As our base data set we use the SDSS NTT/NOT sample introduced in Chapter 5. We remove SNe without a well observed photometric light curve and demand observations both prior and post maximum brightness. After these cuts we are left with 127 spectra. Out of these, 116 spectra have both good host-galaxy subtraction and are of sufficient quality for spectral features to be identified. Finally, we apply a host-galaxy contamination cut of $< 60\%$ in the g-band, motivated by Monte Carlo simulations, which leaves us with 89 spectra.

The SDSS NTT/NOT spectra are compared to a low-redshift reference

sample which consists of three subsets: data from the Harvard-Smithsonian Center for Astrophysics (CfA), the Supernova Cosmology Project (SCP99) and the Online Supernova Spectrum Archive (SUSPECT). Since the NTT and NOT spectra cover the spectral epochs between -9 days and +20, we have only studied reference spectra up to epoch 30.

The CfA sample consists of 162 spectra of 19 SNe Ia from Matheson et al. [86]. The SCP99 data set contains the 79 spectra of 16 SNe observed by the Supernova Cosmology Project in 1999 that were studied by Garavini et al. [43]. The SUSPECT data set collects publicly available SN spectra[1], we use 421 spectra of 40 Type Ia SNe. We will in Section 6.7 also make use of 13 spectra from the high redshift SuperNova Legacy Survey (SNLS) VLT data set presented in Balland et al. [7].

The following analysis relies on SN light curve properties. We have performed SALT and SALT2 fits of the SDSS SNe ourselves, and obtained MLCS fits through the SDSS collaboration (derived using light curves as presented in Holtzman et al. [60]). Light curve fits for the reference samples have been collected from the literature: SALT fits from Kowalski et al. [74] and Hicken et al. [56], SALT2 fits from Amanullah et al. [2], Guy et al. [50] or Arsenijevic et al. [4] and MLCS fits from Hicken et al. [56].[2]

We present in Figure 6.1 the distribution of epoch, redshift, SALT stretch and SALT colour for the NTT/NOT sample together with the main reference samples. Faint SNe, such as those with large light curve colours or observed a month after peak light, can only be observed close to use. This explains why both the epoch and SALT colour distributions differ between local and SDSS SNe. Lists of all spectra and full references are given in Paper C and Paper D.

To note:

- The spectral *epoch* is defined with respect to the peak of the B-band light curve. All spectral epochs used are rest frame epochs and are thus corrected for time dilation.

- The low-z reference sample spectra were *not* host subtracted. These are sufficiently local to allow subtraction of most host galaxy contamination during data reduction.

[1] `http://bruford.nhn.ou.edu/suspect/`.

[2] The SNLS 3yr light curve parameters from Guy et al. [50] rely on an updated version of SALT2, we therefore rescale SNLS SALT2 parameters to match the 64 SNLS SNe that overlap with Amanullah et al. [2]. The uncertainty of this scaling procedure is propagated into the light curve parameter uncertainties.

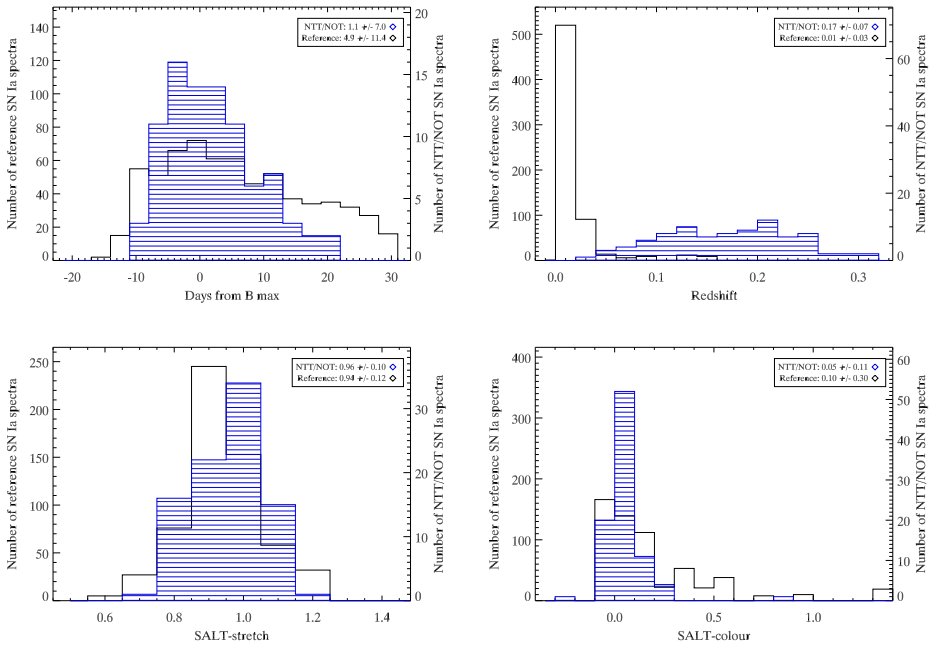

Figure 6.1: Distribution of epoch, redshift, SALT stretch factor and SALT colour for the SN spectra used in our study. The epoch is defined here as the number of days in rest frame from B band maximum brightness. The white histogram is for the reference sample while the striped histogram is for the NTT/NOT spectra used here. Legends show mean and Gaussian 1σ levels for the subsets. Figure from Paper C.

- For pEW studies, spectra are smoothed according to noise level, as described in Section 5.4. For velocity studies, all spectra are binned using bin widths constant in velocity, $c\Delta\lambda/\lambda = 2000$ km s^{-1}.

- The NTT/NOT spectra have well documented uncertainties. However, most of the spectra in the reference sample lack error estimates. For such cases, a constant flux error of 5% of the average spectral flux was used to compute the uncertainties in spectral indicators.

- Systematic uncertainties are estimated from simulations as discussed in Chapter 5. For line velocities, a systematic error of 200 km s^{-1} was included to account for peculiar velocity uncertainties.

6.3 Indicator Change with Epoch

As an initial step we study how spectral indicators evolve with epoch. To allow a visual comparison, the local reference set measurements were combined into 1-σ contours. The first panel of Figure 6.2 illustrates pEW f3 measurements of normal SNe Ia in the reference sample.

Non-normal SNe are displaced with respect to normal, as is e.g. shown in the second panel of Figure 6.2. Note that all known peculiar SNe were removed from the normal reference sample, but that it is in practice impossible to make a strict definition regarding which SNe should be considered as "normal".

Finally, in the third panel of Figure 6.2 we show how NTT/NOT measurements compare with normal local SNe. The samples largely overlap, with a possible tendency for SDSS measurements to lie at the lower one sigma edge. Similar trends are seen for all features, see Paper C for full information. These studies were repeated for line velocities. As an example, the last panel of Figure 6.2 shows the velocity evolution of feature 7 (SiII λ6150) with epoch.

Our ultimate goal is not to study the epoch evolution, but rather how indicators vary with other parameters. We thus remove the epoch dependence through subtracting the average indicator change with epoch (as calculated based on normal reference SNe). After this subtraction we have an *epoch independent* quantity: ΔpEW. In all subsequent analyses this slightly modified pEW will be used.

6.4 Evolution with Redshift

As was discussed in Chapter 4 an undetected evolution in (light curve corrected) SN peak magnitude with redshift would directly bias cosmological parameter estimations. Further, from a theoretical point of view, changing metallicity (and other parameters changing with time, like galaxy ages) could have an impact on SN Ia progenitor composition, but the details remain largely unknown. If the element distribution of the ejecta is affected, this will likely change the observed spectrum [79, 108].

For cosmology, the relevant question is whether the available low-z SN data sets correctly sample the distribution of SNe Ia at cosmological distances. The NTT/NOT data set at intermediate redshifts provides a useful sample relatively nearby but still at cosmological redshifts. Since measurements are done on individual spectra we can potentially distinguish shifting

population demographics (which is expected) from the appearance of new subtypes (not expected and possibly biasing cosmology).

In Paper C we study the evolution of epoch-dependence subtracted indicators, like ΔpEW, with redshift. In some cases we see tentative differences between low and high redshifts. The most interesting results are for pseudo-Equivalent Widths for features 2 and 4 at epochs close to light curve peak. A larger fraction of high-z SNe have small ΔpEWs if compared with the local SNe (see Figure 6.3, grey squares).

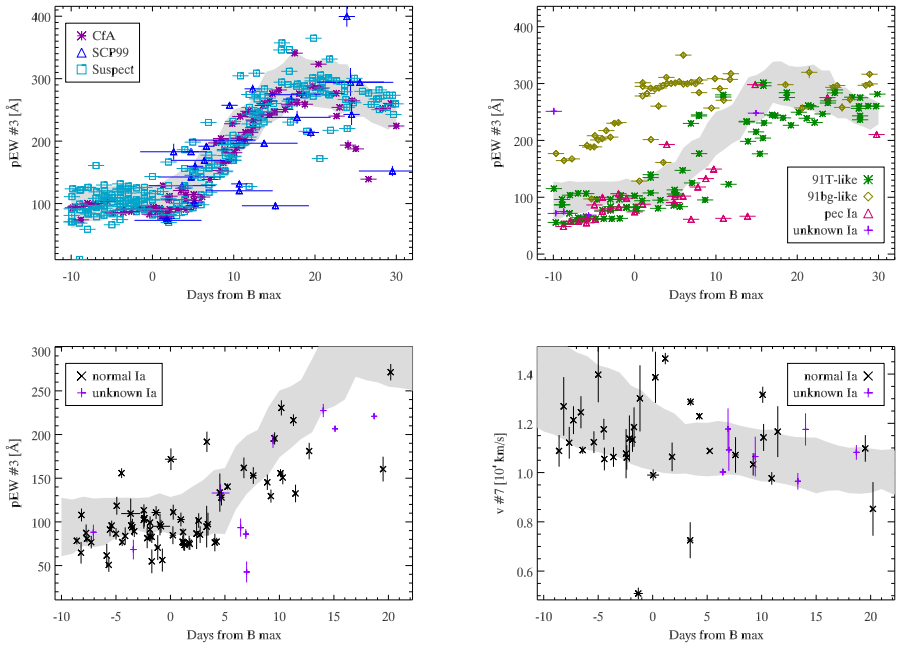

Figure 6.2: *Upper left:* pEW measurements of feature 3 vs epoch for normal low redshift SNe. The shaded region is the average $1-\sigma$ contour based on these measurements. The same average contour is included in the following two panels. *Upper right:* Peculiar SNe, with subtype shown in legend, compared with the normal $1-\sigma$ contour. *Lower left:* Measurements of pEW-f3 for SDSS NTT/NOT SNe, compared with the normal reference $1-\sigma$ contour. Crosses ('+') show SNe identified as possibly peculiar by SNID [15] *Lower right:* Comparisons of line velocities of f7 (SiII λ6150) between the reference sample and the higher redshift SDSS spectra. The shaded band shows the one sigma contour for the normal SNe Ia in the reference sample. Figures from Paper C.

The direction of this evolution agrees with the ESSENCE [38] and SNLS [7, 115] studies of redshift binned composite spectra. Such evolution is what would be expected from changing demographics since e.g. average light curve width increases with redshift in SN surveys [61], and feature widths typically decrease with wider light curves (see Section 6.5).

We can also make a possible link with unidentified peculiar objects. We note that all low redshift SNe with ΔpEW similar to the "deficit" NTT/NOT SNe (grey squares in Figure 6.3 as noted above) are more or less peculiar: SN 2000cx, 2005hk, 2006gz, 1999aw, 1999bp and 1999bn. While the three first of these SNe are very peculiar, the remaining three are "borderline" SN 1991T like or *Shallow Silicon* (SS) SNe Ia (using the terminology of Branch et al. [17]). These subtypes often demand spectra from epochs *before* light curve peak to be securely identified [81]. This is often available for heavily studied local SNe, but not for high redshift objects.

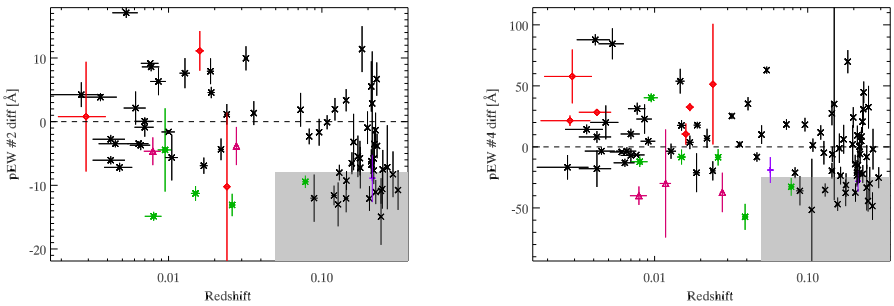

Figure 6.3: Comparison of the ΔpEW measurements (epoch dependence subtracted pEW) vs. redshift for feature 2 (left) and feature 4 (right). Green stars indicate 91T-like, red diamonds 91bg-like and magenta triangles other peculiar SNe. The shaded areas mark regions at higher redshifts were few corresponding *normal* low redshift SNe exist. Spectra within three days of light curve peak are included.

The possible evolution among spectroscopic indicators can thus be explained through a combination of two (connected) effects:

- A fraction of "borderline" peculiar SNe, mainly similar to Shallow Silicon SNe, that would have been identified as such if observed locally. We still do not know if this fraction is evolving.
- Shifting demographics towards brighter SNe with wider light curves and shallower spectral features at high redshifts, caused by both Malmquist

bias and changing galaxy demographics.

With the full SDSS spectroscopic sample we should be able to separate these effects. We do not see any signs of evolution with redshift not compatible with demographic shifts or that would bias SN cosmology.

6.5 Correlations with Light Curve Width

It is well documented that the abundance of SiII is related to the light curve width and thereby the SN luminosity. Nugent et al. [92] introduced the Si-ratio as the ratio of the SiII λ5800 and SiII λ6150 features and showed this to correlate with light curve decline. Similar relations were found for the SiII λ4000 (f2) feature: Garavini et al. [43] studied the breaking-point of the neighbouring f3 feature and Bronder et al. [20] the direct SiII λ4000 correlation with stretch.

This is clearly seen also in the current sample, particularly for the SiII λ4000 feature. While previous studies have been limited to the light curve peak region, we have probed wider epoch ranges (after removing the average epoch dependence).[3] We find the strongest correlations with light curve width for SiII λ4000 in the epoch range -6 to -1. In Figure 6.4 we show both SALT stretch and MLCS Δ comparisons with SiII λ4000 pEW. Both correlations are strong, and linear over large parameter ranges. This supports the idea that spectral indicators can be used as an alternative to photometric properties when calibrating SNe Ia luminosities.

6.6 Correlations with Host Galaxy Properties

The photometric light curves of SNe Ia from different environments exhibit systematic diversity [52]. Since correlations between light curve shape (stretch) and spectral indicators are present in the data analysed, we expect the host-light curve correlation to propagate to a correlation between spectral and host galaxy properties. Recent studies have also found indications of correlations between host galaxy properties, like mass and metallicity, and supernova absolute magnitude, that does *not* appear to be captured by light curve shape or colour [41, 70, 78, 114].

As discussed above, the distribution of SN Ia light curve widths also changes with redshift [61]. These results can be compared with the rates of SNe Ia, and possibly explained by two populations with different properties,

[3] See Paper C for a full discussion of how different epoch ranges are studies.

one "prompt" (number of SNe Ia proportional to host galaxy star formation) and one "delayed" (proportional to host mass instead) [85, 110]. Note that this cannot be the full explanation since it does not explain the SN rate in clusters; all cluster environments are "delayed" and the rate in clusters is still increasing with redshift [8].

Comparisons between spectral indicators and host galaxy properties could potentially help explain why these correlations are seen and what the driving force is.

All SDSS SN host galaxies were studied using the stellar formation code PEGASE. A description of this process can be found in Smith et al. [112] and a comparison with light curve properties and Hubble diagram residuals in Lampeitl et al. [78]. Here we use the estimated host galaxy type, host mass (in units of $M_{\odot}$) and specific Star Formation Rate (sSFR; defined as the star formation rate per stellar mass, yr) and compare with spectral indicators.

As previously, different epoch ranges were probed. Host galaxy type, mass and star formation are highly correlated properties, making it hard to distinguish what is the driving cause for variations with host properties. We find strongest correlation with f2, the SiII λ4000 feature. Figure 6.5 shows some of the most interesting findings. The left panel studies a pre-peak epoch range (-9 to -2), showing how all SNe in massive host galaxies have wide SiII λ4000 absorptions (and narrow light curves). This is consistent with the result that massive early-type galaxies host SNe with narrower light curves. It is interesting that the (very few) SNe in massive hosts indicates a separate subgroup.

A second sample result is shown in the right panel of Figure 6.5. We here study spectra in the epoch range $0 - 8$ and compare SiII λ4000 widths with specific Star Formation Rate. Once more we find, consistent with earlier results, that the star forming (less massive) galaxies have narrower SiII λ4000 widths, possibly with a tendency for subgroups here as well. Surprisingly we also find that SNe from star forming galaxies have bluer SALT light curve colours. We would expect these SNe to experience more dust reddening and thus have redder colours. We will in the next section continue the discussion regarding the SiII λ4000 feature and light curve colour.

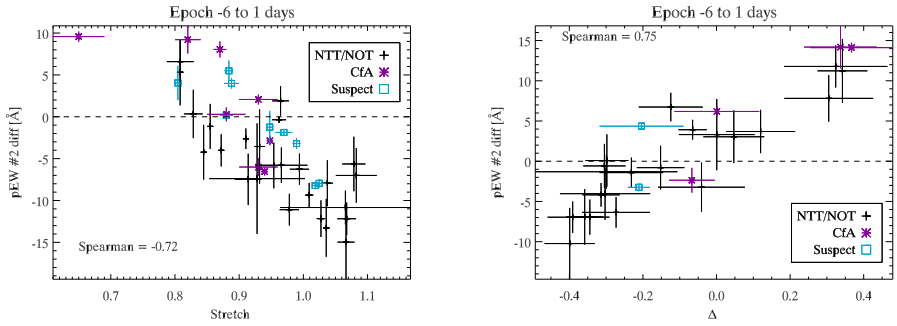

Figure 6.4: Figures show how SiII λ4000 ΔpEW (epoch independent pEW) varies with light curve width: stretch (SALT output) in the left panel and Δ (MLCS output) in the right. Spectra of normal SNe in the epoch range (-6 to -1) are included. The panels also include the Spearman rank correlation coefficient and the origin of the data. Figure from Paper C.

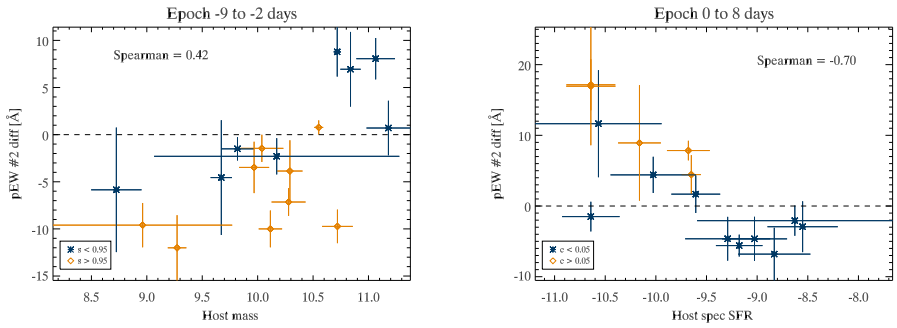

Figure 6.5: pseudo-Equivalent Width of feature 2 (SiII λ4000) compared with host galaxy properties. *Left panel:* Host mass for pre peak epochs (-9 to 2) with symbols marking low/high light curve stretch SNe. *Right panels:* Specific Star Formation Rate for post peak epochs (0 to 8) with symbols marking low/high light curve colour SNe. Figure from Paper C.

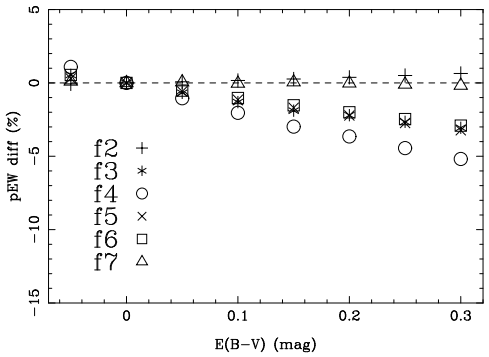

Figure 6.6: Percent change in pEW for features 2 to 7 as a function of E(B−V). The measurements are based on the Hsiao et al. [64] SN template at peak brightness and assuming Cardelli et al. [22] type dust with $R_V = 1.7$. Figure from Paper C.

6.7 Si*II* λ4000 and Light Curve Colour

6.7.1 Introduction

That SNe Ia are found to be more or less "reddened", and that such an effect is expected from dust extinction in the host galaxy, was discussed in Section 3.2.1. However, the colour-brightness relation of SNe Ia does not seem to match the Milky-Way dust extinction law, instead preferring a "steeper" law (lower R_V) [1, 5, 48, 76, 90, 101, 103, 119]. Some well measured SNe are better fitted with a much steeper extinction law, as would be produced by circumstellar material [37, 44]. Further, how reddening is accounted for is one of the major systematic uncertainties in current SN cosmology (Paper A).

It is therefore of great interest whether any spectroscopic indicators are correlated with SN colour (beyond what is expected from Δm_{15} - $E(B-V)$ correlations). Line velocities and pEWs are only very mildly affected by Milky-Way type dust extinction (see Figure 6.6), and any significant observed correlation would imply that at least some reddening is intrinsic to the SN system. Thus, comparisons of spectra of SNe with different colours may help in the understanding of the intrinsic colour dispersion in SNe Ia and allow us to disentangle the various components entering the colour-brightness relation.

6.7.2 SiII λ4000 pEW and SALT2

In a blind search for correlations between spectral properties and light curve colour (as estimated by SALT), we found in Paper C that the SiII λ4000 pEW in the epoch range 0-8 displays a statistically significant correlation with SALT c.[4] To probe the significance of this correlation, Paper D examines the same epoch range but using the SALT2 c (colour) parameter and including new, independent, SN spectra from the SuperNova Legacy Survey observed at VLT [7].[5]

In Figure 6.7 sample SNe with narrow and wide SiII λ4000 features are shown.[6] The correlation found would imply that SNe with smaller pEW have bluer light curve colours. In Figure 6.8 we compare SiII λ4000 ΔpEW measurements for all SNe with spectra with epochs (0-8) that also have SALT2 colour fits in the combined SDSS/local/SNLS sample. The Spearman correlation coefficient for the correlation is 0.67, which for the 55 objects corresponds to a rejection of the non-correlation hypothesis at the 5.8 σ level.[7] If the most reddened SNe are removed ($c > 0.3$), the significance changes to 5.2 σ. We cannot with this limited sample differentiate between a continuous correlation or different subclasses, but note that all measurements with $c < 0.25$ follow a fairly linear trend (pEW-c) while redder SNe do not.

The *Branch-types* were introduced as a qualitative subtyping scheme by Branch et al. [17, 18][8] Among the 20 SNe with determined Branch type, all were classified as either Core Normal (CN) or Broad Line (BL). There are no Cool or Shallow Silicon SNe, consistent with a sample only consisting of normal SNe Ia. Among the 14 moderately reddened ($c \lesssim 0.3$) SNe with

[4]Note that several studies (including Paper C) have looked for relations between pEWs and light curve colours at light curve *peak* without finding any significant correlations. It is essential, and not surprising, that specific epoch ranges have to be probed.

[5]Reminder: The c parameter describes an empirically fit wavelength dependent flux attenuation. SNe with high c-values are "redder" in the sense of having less flux at short wavelengths, while SNe with small c-values can be called "bluer".

[6]The SiII λ4000 region is complex: While Si absorption dominates, many SNe display small additional absorption by additional elements. Various authors have suggested absorption by CII, CrII, CoII or FeIII in this region, e.g. [18, 42, 109, 118].

[7]Spearman's rank correlation coefficient is similar to the Pearson correlation coefficient but relies on ranked variables (making it more suitable for non-Gaussian distributed measurements). The output coefficient range from −1 to 1, with 0 meaning no correlation. See Section 5.1 in Paper C for further details.

[8]This is a classification scheme based on the shape of the SiII λ5800 and SiII λ6150 features: normal "Core Normal" (CN), broader "Broad Line" (BL), weaker "Shallow Silicon" (SS) or with the deep absorptions of fainter SNe Ia, "Cool".

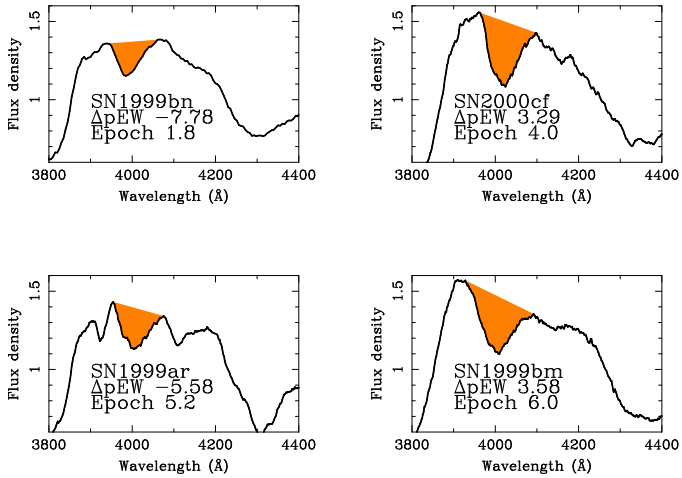

Figure 6.7: *The SiII λ4000 feature of SNe Ia.* Top left: SN1999bn at day +2 (SiII λ4000 ΔpEW= −7.78 Å). Top right: SN2000cf at day +4 (ΔpEW= 3.29 Å). Bottom left: SN1999ar at day +5 (ΔpEW= −5.58 Å). Bottom right: SN1999bm at day +6 (ΔpEW=3.58 Å). Left panels show SNe with narrow SiII λ4000 feature also after removing epoch dependence, while right panel SNe have wider Si II λ 4000. Figure from Paper D.

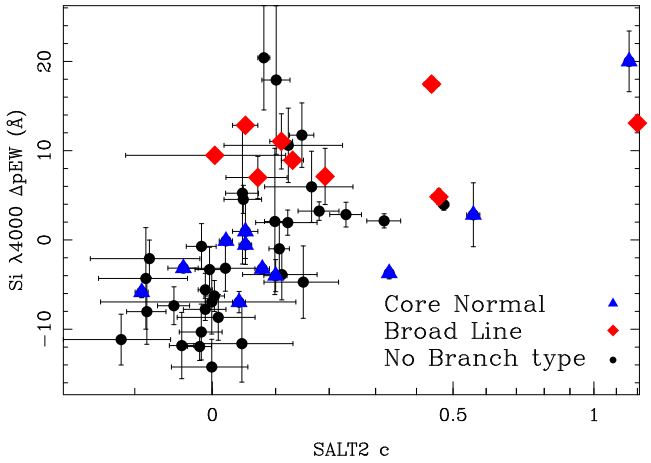

Figure 6.8: *SiII λ4000 ΔpEW vs.* SALT2 *c with the Branch classes marked using different symbols.* The X-axis is displayed with logarithmic intervals for clarity (see Paper D for a non-logarithmic version of this Figure).

Branch-typing, all SNe with wide SiII λ4000 (ΔpEW$\gtrsim$ 3 Å) are Broad Line SNe, while all with narrow SiII λ4000 (ΔpEW$\lesssim$ 3 Å) are Core Normal.

We have investigated a range of possible systematic effects that could create a pEW-colour correlation, these are further described in Paper C and Paper D. Different subsamples, with varying noise and host contamination issues, all yield consistent results and no subsample is driving the trend. Monte Carlo runs show that standard dust reddening would not cause the behaviour seen. In summary, we cannot find any systematic effect that would explain the correlation between SiII λ4000 pEW and SALT2 colour in Figure 6.8.

To further understand the SiII λ4000 region of SNe Ia we have studied how ΔpEW measurements vary with the SiII λ6150 *velocity gradient*, the average change in SiII λ6150 line velocity with epoch. Benetti et al. [10] studied the velocity gradients of local SNe and used this quantity to classify SNe as high velocity gradient (HVG), low velocity gradient (LVG) or Faint. HVG and LVG SNe have similar light curve widths but different expansion evolution, thus showing that SNe Ia cannot be completely described by the light curve width.

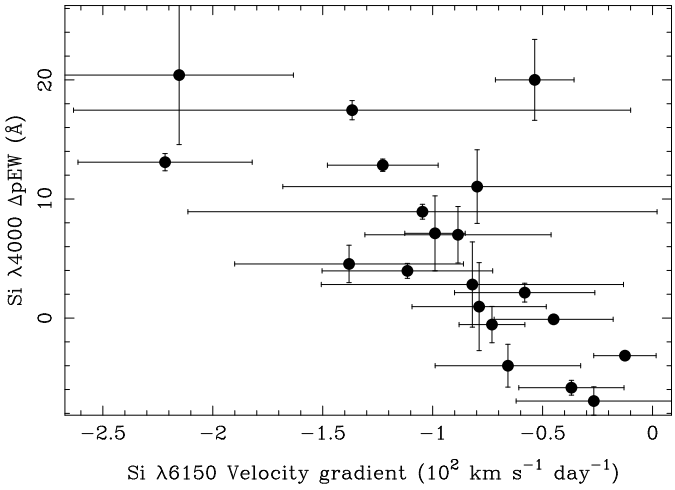

Figure 6.9: *SiII λ4000 ΔpEW vs. velocity gradient of SiII λ6150.* This is defined as the slope of a linear fit of velocity decrease per unit time (km s^{-1} day^{-1}). We require at least three spectra within epoch −7 to +20 so that also an uncertainty can be estimated.

In Figure 6.9 we compare SiII λ4000 ΔpEW measurements with the SiII λ6150 velocity gradient for the 22 SNe with three or more spectra in the

rest frame epoch range −7 to +20 (the range where the SiII λ6150 velocity typically is well defined). There is a strong correlation (at the 3.8 to 4.3 σ level) where SNe with wider SiII λ4000 features have steeper velocity gradients, thus faster photospheric velocity evolution.

6.7.3 SiII λ4000 Discussion

The tentative results discussed here can be connected with a number of different recent studies of other spectroscopic properties. Maeda et al. [84] argue that the velocity gradient is related to shifts in nebular line velocities and that this can be explained through viewing angle effects from a non-symmetric explosion. Wang et al. [124] use a sample divided according to high or low SiII λ6150 velocity to obtain either different extinction laws or different intrinsic colours. The Supernova Factory collaboration has claimed both that flux ratios can provide better peak magnitude corrections than what light curve properties yield [6] and that after corrections based on *two* pEWs, SiII λ4000 and CaII H&K, any remaining reddening resembles Milky Way-type dust extinction [24].

These findings imply that the observed (light curve) colours of SNe are *at least* caused by *two* physical processes: one local to the SN and then additional absorption by host galaxy dust (which must exist at some level). It would be a strange coincidence if these processes yield identical extinction laws, and it is therefore likely that SN light curve fitters would yield better cosmological constraints if these mechanisms were taken into account separately.

When trying to understand these correlations it is important to differentiate between "physical" colour and "light curve" colour: A "physical" colour is the difference between two measured magnitudes in different filters (e.g. B-V). Physical colours are correlated with the light curve decline rate [98]. A "light curve" colour is the estimated total "colour" by a light curve fitter, in this case SALT or SALT2. The latter entity depends on the model used by the light curve fitter. Since we are studying SNe at different redshifts, observed using different filters, we are forced to use a light curve fitted colour. Light curve fitters like SALT2 attempt to describe all first order intrinsic light curve shape effects (width *and* colour) with the x_1 parameter, leaving the light curve colour parameter c as an external empirical extinction.

The tentative SiII λ4000 correlations presented above, if confirmed, would provide a mechanism to distinguish different intrinsic (SALT2) "colours". We have, for the small SiII λ4000 sample in the Hubble Flow ($z > 0.02$),

compared peak luminosities with SiII λ4000 pEW, see Figure 6.10. The data are sparse, but it is possible that two different behaviours exist: SNe with narrow SiII λ4000 regions exhibit a pEW - magnitude correlation, which could be alternatively described as a reddening - magnitude correlation. SNe with large ΔpEW (ΔpEW$\gtrsim$ 3 Å) show a small magnitude scatter that is not improved through light curve colour corrections. More data are needed to study such effects.

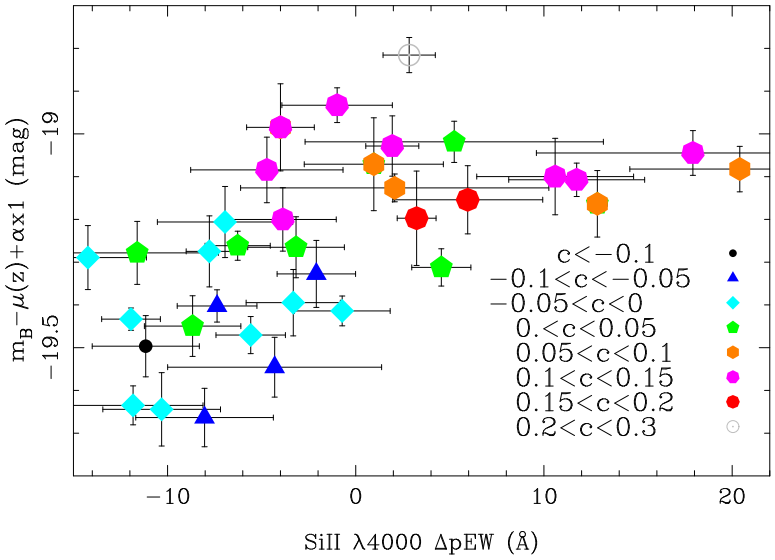

Figure 6.10: ΔpEW *vs. distance and light curve width corrected magnitude.* SNe are marked according to SALT2 c (colour). Only SNe in the Hubble flow ($z > 0.02$) are included. A distance modulus, $\mu(z)$, has been subtracted from all magnitudes, assuming a flat ΛCDM cosmology with $\Omega_M = 0.27$. Magnitudes were also corrected for light curve width, x_1, assuming the α best fit value from Union2 ($\alpha = 0.121$).

Two observational remarks can be made regarding the SiII λ4000 feature. (i) Measurements can be made up to high redshifts since signal-to-noise requirements are moderate and the feature is not redshifted into the IR. (ii) Measurements of pEWs do not require spectro-photometric data (like flux ratios), and are thus feasible with e.g. multi-fibre spectroscopy (provided host contamination levels are not too high).

Chapter 7

Summary and Outlook

Our knowledge of Type Ia supernovae is rapidly increasing. We are now really probing traditional "big" unknowns, like the nature of the progenitor and the source of reddening. This progress should allow us to standardise SNe Ia even further, providing sharper constraints on dark energy properties. In the next few years we hope to device methods allowing a further leap forward.

The work presented in this thesis is intended to be a (small) part of this development. Paper A introduces `SMOCK`, a framework designed to study a wide range of different systematic uncertainties. We need to show that the upper limits on these uncertainties really translates into small uncertainties on cosmological parameter estimates.

The main part of this thesis is devoted to quantitative studies of properties of SNe Ia spectra. These are made possible by the large amount of spectra currently available and made necessary by the lower signal-to-noise levels in each individual spectrum. The SDSS NTT/NOT sample (Paper B) provides one opportunity for such studies. It is obtained at an advantageous redshift range, where evolution and new subtypes can be expected but not so distant that spectra cannot be examined on an individual basis.

A large combined spectroscopic sample, including both NTT/NOT and local SNe, have allowed us to study correlations between spectral indicators and global SN properties (Papers C and D). Properties of the explosion are directly seen in the SN spectrum, and can be connected to both the light curve width and possibly the colour. We have studied evolution with redshift, and found tentative changes, compatible with what is expected from changing demographics. Correlations with host galaxy properties are also interesting, but limited by the small sample available.

7.1 Outlook

The work presented here can, and is being, extended in several ways.

The studies of spectral indicators can be increased through the addition of the full SDSS spectroscopic sample. It would then also be possible to take advantage of the currently ongoing studies of the host galaxies of SDSS supernovae. This will allow us both to achieve better host galaxy subtraction of SN spectra as well as giving better measured host galaxy properties with which to compare the SNe.

The old discussion regarding the nature of reddening will also be continued, and one way forward could be to try to understand how colour, spectroscopic indicators and signs of SN asymmetry (nebular line shifts) interact. Another important future task is to study what implications recent lessons from spectroscopy have on future huge photometric surveys. Could photometry alone, complemented with e.g. IR observations, yield not only accurate typing but also an improved SN standardisation?

Finally, we would like to observe ever more distant SNe! One very exciting way to do so is through using the gravitational magnification provided by massive clusters. We are currently looking for magnified distant SNe behind several such clusters. Besides interesting high redshift SNe (of all types) we will also be able to determine the rate of SNe at very high redshifts, which in turn provides constraints on both the star formation history and on the progenitors of SNe.

Chapter 8

Astronomical Terms

Spectrum, photometry, filter, reduction Objects in the universe emit signals. Electromagnetic radiation, photons, are the most easily observed such. The recorded intensity of light from a target as a function of photon wavelength is called a *spectrum*. Spectroscopy is very inefficient, both because light only through a one-dimensional slit is observed and because photons are lost when separated according to frequency. To improve efficiency all photons, irrespectively of frequency, from a 2-dimensional patch of the sky can be observed (called *photometry*). Usually a *filter* is used, accepting photons in some frequency range and thus providing some information regarding the nature of the observed light. Several filter-systems have been defined.

In Figure 8.1 we display a spectrum of a Type Ia supernova, together with the transmission curves for the Bessel 'U','B','V','R' and 'I' filters. Photometry in the 'B'-band will thus yield the convolved flux of the spectrum and the 'B'-filter transmission curve.

Raw data needs to be calibrated before usage (taking for example the sensitivity of the CCD into account). This process is commonly denoted *reduction*.

Magnitude, colour For historical reasons luminosities are usually given as magnitudes, that is the logarithm of the flux: $m_{\text{filter}} = -2.5 \cdot log(\text{flux}_{\text{filter}}) + Z_P$. Note that brighter objects have lower magnitudes and that to properly "understand" a magnitude we need to know both through which filter it was observed and how the zero point (Z_P) was defined. With a *colour* we mean the difference between the magnitudes in two filters, e.g. $B - V$ (it is thus really the ratio between flux at different wavelengths). Usually the "bluer"

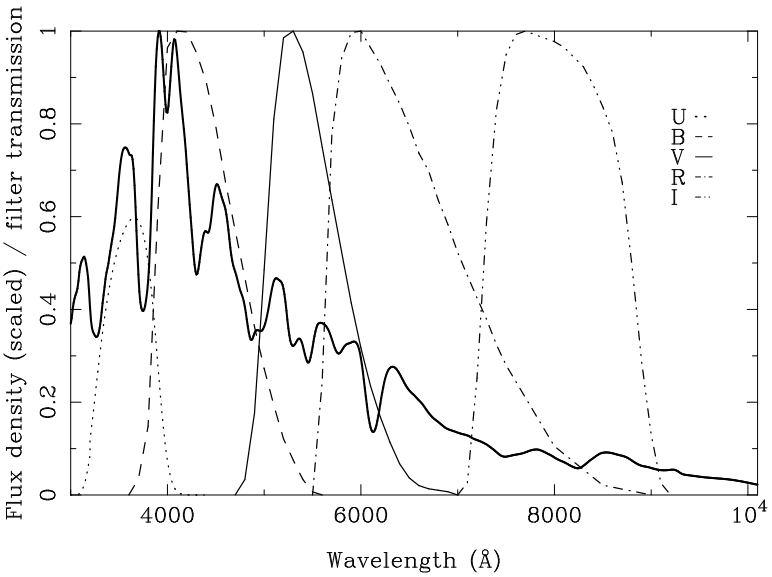

Figure 8.1: A sample *spectrum* (template SNe Ia from [64]). The Bessel 'U','B','V','R' and 'I' *filter* transmission wavelengths are overlaid.

filter is written first, implying that a larger colour means a "redder" object, hence the term *colour*.

Redshift, rest frame Frequencies change with relative motion. For example, if a source emitting light is moving towards the observer the observed frequency will be higher (shorter wavelength) than what was emitted. Since the universe is expanding astronomical objects are seen as moving away from us, and light will thus be *redshifted* to longer wavelengths. This is usually described through the z parameter: $z = (\lambda_{obs} - \lambda_{emit})/\lambda_{emit} = (f_{emit} - f_{obs})/f_{obs}$. Since more distant objects are moving "faster away" the redshift gives (one!) measure of the distance - objects with higher redshifts are more distant and we observe them at a time when the universe was younger. Light observed by us will be at observer wavelengths, if we correct wavelengths to these emitted by the source (using the formula above) we obtain *rest frame* wavelengths.

Differential atmospheric refraction, slit loss, parallactic angle *Slit loss* occurs when not all light from an object enters the slit through which the spectrum is observed. One source of slit loss is *Differential Atmospheric Refraction* (DAR), an effect caused by the wavelength-dependant refraction

index of air, that causes spectra observed through the atmosphere to suffer wavelength dependant losses. A spectrum is observed through a thin slit and as the refraction of air will cause photons to be dispersed along the *parallactic angle* (the angle normal to the horizon), according to wavelength, only photons of one frequency will land exactly in the slit. Away from this more and more photons will "miss" the slit. This effect will increase in magnitude as objects are observed closer to the horizon (through more atmosphere). DAR can be avoided if the slit is placed along the parallactic angle.

Chapter 9

Summary for the General Audience

A *supernova* signals the violent end of a star. We see it as a bright new point of light, visible for a few weeks. Stars come in all sorts of types and sizes, as do supernovae. One of these types are the *Type Ia supernovae*. This is a special type for example since they do not show any traces of Hydrogen or Helium, the otherwise most common elements in the universe. Another remarkable fact is that they always seem to be equally bright - whenever we detect a Type Ia supernova we know how bright it really is. They are *standard candles*.

This fact can be used to study the expansion of the universe. Scientists have devised a very good description of the universe. This starts with the Big Bang, from which everything has been expanding from everything else, ever since. But we do not know if and how long this will continue. We can use standard candles to measure this as follows: If we study several candles at different distances and measure how bright they *seem to us* we can calculate how much the universe must have expanded between these distances. Slightly more than a decade a ago it was discovered that Type Ia supernovae far away from us are fainter than they "should be". The only way to explain this is through a new energy source driving an accelerated expansion of the Universe. This source, whatever it is, was dubbed *dark energy*.

The work presented in this thesis starts with an examination of how sensitive our measurements of dark energy, using supernovae, are to a range of *systematic uncertainties*. This is discussed in Chapter 4 which is in turn based on Paper A. Systematic uncertainties, like calibration and that Type

Ia supernovae are not perfect standard candles, are what currently limits what we can say regarding the properties of dark energy (using supernova measurements). We find that the dominant astrophysical uncertainties come from (i) that some supernovae are redder than others and (ii) that we can not fully rule out that supernovae evolve with time. To limit these, and thus determine exactly what this mysterious dark energy is, we simply have to understand Type Ia supernovae better. We, in fact, don't even know exactly what it is that explodes...

One way to learn more about supernovae is to study spectra, recordings of how the light from a supernova varies in strength with the frequency of the light (see Figure 3.5). In Chapter 5 (and Paper B) we describe the *SDSS NTT/NOT* sample of spectra of supernovae. These were observed at two telescopes in 2006 and 2007. We have been working with the calibration of the raw data and the typing (determining what kind of object is actually observed).

After this, Chapter 6 (and Papers C and D) explores how we can use spectra of supernovae to learn more about them. We do this by measuring *spectral indicators* (the size and position of the wiggles in the Figure 3.5). With these measurements we can study for example the physics of the explosion (the depth of features vary with temperature), evolution with time/distance (we do not see any unexpected evolution) and the reddening effect. Dust in the host galaxy will cause some Type Ia supernovae to look redder than others, but it now seems like there must be some other, additional, source of reddening.

Acknowledgements

A humongous *Thank You*, complete with trumpets, choirs and jingle bells, to everyone that has supported, guided, entertained, annoyed and rescued me during the last five years!

I have grown and worked in the protective SNOVA environment. First of all, thanks to Ariel, who besides being an excellent supervisor never ceases to conjure new worthy ideas (to be investigated all at once). Rahman, whether you are conscious of it or not, I have learned most of what I know from you (including not to dance without warm-up). Linda, I have enjoyed our cooperation immensely (possibly excluding the time spent in the shadow of Bloukrans bridge), and I would not have carried these projects through without you. The list of important SNOVAers continues: Jacke, Joel, Edvard, Serena, Kerstin...

As always, more people deserve to be mentioned than there is space. To all my colleagues: I am constantly impressed by the vast scope of what you know and do. I still hope to be able to understand at least a fraction some day! And to all my friends, wherever you are: Don't stop asking how my astrology is coming along! I only wish we had more time together.

I realise more and more how much my family (including the growing German side) has meant, and continues to mean, to me. I am very very lucky to have you all and I hope I can repay you for your unwavering support.

Pancha - you have the most wonderful way to disentangle my brain.

Bibliography

[1] Altavilla, G., G. Fiorentino, M. Marconi, et al., 2004, MNRAS, 349, 1344

[2] Amanullah, R., C. Lidman, D. Rubin, et al., 2010, ApJ, 716, 712

[3] Arnett, W. D., 1982, ApJ, 253, 785

[4] Arsenijevic, V., S. Fabbro, A. M. Mourão, and A. J. Rica da Silva, 2008, A&A, 492, 535

[5] Astier, P., J. Guy, N. Regnault, et al., 2006, A&A, 447, 31

[6] Bailey, S., G. Aldering, P. Antilogus, et al., 2009, A&A, 500, L17

[7] Balland, C., S. Baumont, S. Basa, et al., 2009, A&A, 507, 85

[8] Barbary, K., G. Aldering, R. Amanullah, et al., 2010, ArXiv e-prints

[9] Baumont, S., C. Balland, P. Astier, et al., 2008, A&A, 491, 567

[10] Benetti, S., E. Cappellaro, P. A. Mazzali, et al., 2005, ApJ, 623, 1011

[11] Bergström, L., M. Goliath, A. Goobar, and E. Mörtsell, 2000, A&A, 358, 13

[12] Bergström, L. and A. Goobar, Cosmology and particle astrophysics. (1999)

[13] Blomqvist, M. and E. M ortsell, 2010, Journal of Cosmology and Astro-Particle Physics, 5, 6

[14] Blondin, S., L. Dessart, B. Leibundgut, et al., 2006, AJ, 131, 1648

[15] Blondin, S. and J. L. Tonry, 2007, ApJ, 666, 1024

[16] Branch, D., L. C. Dang, and E. Baron, 2009, PASP, 121, 238

[17] Branch, D., L. C. Dang, N. Hall, et al., 2006, PASP, 118, 560

[18] Branch, D., D. J. Jeffery, J. Parrent, et al., 2008, PASP, 120, 135

[19] Bravo, E., L. G. Althaus, E. García-Berro, and I. Domínguez, 2011, A&A, 526, A26+

[20] Bronder, T. J., I. M. Hook, P. Astier, et al., 2008, A&A, 477, 717

[21] Burns, C. R., M. Stritzinger, M. M. Phillips, et al., 2011, AJ, 141, 19

[22] Cardelli, J. A., G. C. Clayton, and J. S. Mathis, 1989, ApJ, 345, 245

[23] Chandrasekhar, S., 1935, MNRAS, 95, 207

[24] Chotard, N., E. Gangler, G. Aldering, et al., 2011, A&A, 529, L4+

[25] Conley, A., J. Guy, M. Sullivan, et al., 2011, ApJS, 192, 1

[26] Conley, A., M. Sullivan, E. Y. Hsiao, et al., 2008, ApJ, 681, 482

[27] Contardo, G., B. Leibundgut, and W. D. Vacca, 2000, A&A, 359, 876

[28] Cumming, R. J., P. Lundqvist, L. J. Smith, M. Pettini, and D. L. King, 1996, MNRAS, 283, 1355

[29] Dahlen, T., B. Mobasher, S. Jouvel, et al., 2008, AJ, 136, 1361

[30] Dekker, H., B. Delabre, and S. D'Odorico, in Crawford, D. L., editor, Society of Photo-Optical Instrumentation Engineers (SPIE) Conference Series, vol. 627 of *Society of Photo-Optical Instrumentation Engineers (SPIE) Conference Series* (1986)

[31] Di Stefano, R., R. Voss, and J. S. W. Claeys, 2011, ArXiv e-prints

[32] Ellis, R. S., M. Sullivan, P. E. Nugent, et al., 2008, ApJ, 674, 51

[33] Filippenko, A. V., 1997, ARA&A, 35, 309

[34] Filippenko, A. V., T. Matheson, and L. C. Ho, 1993, ApJL, 415, L103+

[35] Filippenko, A. V., M. W. Richmond, D. Branch, et al., 1992, AJ, 104, 1543

[36] Folatelli, G., 2004, Type Ia Supernova Cosmology: Quantitative Spectral Analysis, Ph.D. thesis, Stockholm University, Stockholm, Sweden

[37] Folatelli, G., M. M. Phillips, C. R. Burns, et al., 2010, AJ, 139, 120

[38] Foley, R. J., A. V. Filippenko, C. Aguilera, et al., 2008, ApJ, 684, 68

[39] Fransson, F., 2006, Lecture notes in High Energy Astrophysics

[40] Frieman, J. A., B. Bassett, A. Becker, et al., 2008, AJ, 135, 338

[41] Gallagher, J. S., P. M. Garnavich, N. Caldwell, et al., 2008, ApJ, 685, 752

[42] Garavini, G., G. Aldering, A. Amadon, et al., 2005, AJ, 130, 2278

[43] Garavini, G., G. Folatelli, S. Nobili, et al., 2007, A&A, 470, 411

[44] Goobar, A., 2008, ApJL, 686, L103

[45] Goobar, A., L. Bergström, and E. Mörtsell, 2002, A&A, 384, 1

[46] Goobar, A. and B. Leibundgut, 2011, ArXiv e-prints

[47] Goobar, A., E. Mörtsell, R. Amanullah, et al., 2002, A&A, 392, 757

[48] Guy, J., P. Astier, S. Baumont, et al., 2007, A&A, 466, 11

[49] Guy, J., P. Astier, S. Nobili, N. Regnault, and R. Pain, 2005, A&A, 443, 781

[50] Guy, J., M. Sullivan, A. Conley, et al., 2010, A&A, 523, A7+

[51] H. Karttunen, P. Krüger, H. Oja, M. Poutanen, & K. J. Donner , editor, 2007, Fundamental Astronomy (2007)

[52] Hamuy, M., M. M. Phillips, N. B. Suntzeff, et al., 1996, AJ, 112, 2391

[53] Hamuy, M., M. M. Phillips, N. B. Suntzeff, et al., 1996, AJ, 112, 2398

[54] Hayden, B. T., P. M. Garnavich, D. Kasen, et al., 2010, ApJ, 722, 1691

[55] Hicken, M., P. M. Garnavich, J. L. Prieto, et al., 2007, ApJL, 669, L17

[56] Hicken, M., W. M. Wood-Vasey, S. Blondin, et al., 2009, ApJ, 700, 1097

[57] Hillebrandt, W. and J. C. Niemeyer, 2000, ARA&A, 38, 191

[58] Hoeflich, P., J. C. Wheeler, and F. K. Thielemann, 1998, ApJ, 495, 617

[59] Hoflich, P., A. M. Khokhlov, and J. C. Wheeler, 1995, ApJ, 444, 831

[60] Holtzman, J. A., J. Marriner, R. Kessler, et al., 2008, AJ, 136, 2306

[61] Howell, D. A., M. Sullivan, A. Conley, and R. Carlberg, 2007, ApJL, 667, L37

[62] Howell, D. A., M. Sullivan, P. E. Nugent, et al., 2006, Nature, 443, 308

[63] Howell, D. A., M. Sullivan, K. Perrett, et al., 2005, ApJ, 634, 1190

[64] Hsiao, E. Y., A. Conley, D. A. Howell, et al., 2007, ApJ, 663, 1187

[65] Jha, S., A. G. Riess, and R. P. Kirshner, 2007, ApJ, 659, 122

[66] Jönsson, J., T. Kronborg, E. Mörtsell, and J. Sollerman, 2008, A&A, 487, 467

[67] Justham, S., 2011, ApJL, 730, L34+

[68] Kasen, D., 2010, ApJ, 708, 1025

[69] Kasen, D. and T. Plewa, 2007, ApJ, 662, 459

[70] Kelly, P. L., M. Hicken, D. L. Burke, K. S. Mandel, and R. P. Kirshner, 2010, ApJ, 715, 743

[71] Kessler, R., A. C. Becker, D. Cinabro, et al., 2009, ApJS, 185, 32

[72] Kim, A., A. Goobar, and S. Perlmutter, 1996, PASP, 108, 190

[73] Konishi, K., D. Cinabro, P. M. Garnavich, et al., 2011, ArXiv e-prints

[74] Kowalski, M., D. Rubin, G. Aldering, et al., 2008, ApJ, 686, 749

[75] Kozma, C., C. Fransson, W. Hillebrandt, et al., 2005, A&A, 437, 983

[76] Krisciunas, K., N. C. Hastings, K. Loomis, et al., 2000, ApJ, 539, 658

[77] Lampeitl, H., R. C. Nichol, H. Seo, et al., 2010, MNRAS, 401, 2331

[78] Lampeitl, H., M. Smith, R. C. Nichol, et al., 2010, ApJ, 722, 566

[79] Lentz, E. J., E. Baron, D. Branch, P. H. Hauschildt, and P. E. Nugent, 2000, ApJ, 530, 966

[80] Li, W., A. V. Filippenko, R. Chornock, et al., 2003, PASP, 115, 453

[81] Li, W., J. Leaman, R. Chornock, et al., 2011, MNRAS, 412, 1441

[82] Lidman, C., D. A. Howell, G. Folatelli, et al., 2005, A&A, 430, 843

[83] Linder, E. V., 2006, Astroparticle Physics, 26, 102

[84] Maeda, K., S. Benetti, M. Stritzinger, et al., 2010, Nature, 466, 82

[85] Mannucci, F., M. Della Valle, N. Panagia, et al., 2005, A&A, 433, 807

[86] Matheson, T., R. P. Kirshner, P. Challis, et al., 2008, AJ, 135, 1598

[87] Mattila, S., P. Lundqvist, J. Sollerman, et al., 2005, A&A, 443, 649

[88] Mazzali, P. A., K. Nomoto, E. Cappellaro, et al., 2001, ApJ, 547, 988

[89] Minkowski, R., 1941, PASP, 53, 224

[90] Nobili, S. and A. Goobar, 2008, A&A, 487, 19

[91] Nugent, P., A. Kim, and S. Perlmutter, 2002, PASP, 114, 803

[92] Nugent, P., M. Phillips, E. Baron, D. Branch, and P. Hauschildt, 1995, ApJL, 455, L147+

[93] Östman, L. and E. Mörtsell, 2005, Journal of Cosmology and Astro-Particle Physics, 2, 5

[94] Patat, F., S. Benetti, E. Cappellaro, et al., 1996, MNRAS, 278, 111

[95] Perlmutter, S., G. Aldering, G. Goldhaber, et al., 1999, ApJ, 517, 565

[96] Phillips, M. M., 1993, ApJL, 413, L105

[97] Phillips, M. M., W. Li, J. A. Frieman, et al., 2007, PASP, 119, 360

[98] Phillips, M. M., P. Lira, N. B. Suntzeff, et al., 1999, AJ, 118, 1766

[99] Phillips, M. M., L. A. Wells, N. B. Suntzeff, et al., 1992, AJ, 103, 1632

[100] Podsiadlowski, P., P. A. Mazzali, P. Lesaffre, C. Wolf, and F. Forster, 2006, ArXiv Astrophysics e-prints

[101] Reindl, B., G. A. Tammann, A. Sandage, and A. Saha, 2005, ApJ, 624, 532

[102] Riess, A. G., A. V. Filippenko, P. Challis, et al., 1998, AJ, 116, 1009

[103] Riess, A. G., W. H. Press, and R. P. Kirshner, 1996, ApJ, 473, 588

[104] Riess, A. G., L.-G. Strolger, S. Casertano, et al., 2007, ApJ, 659, 98

[105] Röpke, F. K., W. Hillebrandt, W. Schmidt, et al., 2007, ApJ, 668, 1132

[106] Ruiz-Lapuente, P., F. Comeron, J. Méndez, et al., 2004, Nature, 431, 1069

[107] Sako, M., B. Bassett, A. Becker, et al., 2008, AJ, 135, 348

[108] Sauer, D. N., P. A. Mazzali, S. Blondin, et al., 2008, MNRAS, 391, 1605

[109] Scalzo, R. A., G. Aldering, P. Antilogus, et al., 2010, ApJ, 713, 1073

[110] Scannapieco, E. and L. Bildsten, 2005, ApJL, 629, L85

[111] Schlegel, D. J., D. P. Finkbeiner, and M. Davis, 1998, ApJ, 500, 525

[112] Smith, M., H. Lampeitl, and others, 2011, to be submitted

[113] Sollerman, J., E. Mörtsell, T. M. Davis, et al., 2009, ApJ, 703, 1374

[114] Sullivan, M., A. Conley, D. A. Howell, et al., 2010, ArXiv e-prints 1003.5119

[115] Sullivan, M., R. S. Ellis, D. A. Howell, et al., 2009, ApJL, 693, L76

[116] Swartz, D. A., A. Clocchiatti, R. Benjamin, D. F. Lester, and J. C. Wheeler, 1993, Nature, 365, 232

[117] Taubenberger, S., S. Hachinger, G. Pignata, et al., 2008, MNRAS, 385, 75

[118] Thomas, R. C., G. Aldering, P. Antilogus, et al., 2007, ApJL, 654, L53

[119] Tripp, R., 1998, A&A, 331, 815

[120] Truran, J. W., W. D. Arnett, and A. G. W. Cameron, 1967, Canadian Journal of Physics, 45, 2315

[121] Wald, R. M., General relativity (1984)

[122] Walker, E. S., I. M. Hook, M. Sullivan, et al., 2011, MNRAS, 410, 1262

[123] Wang, L. and J. C. Wheeler, 2008, ARA&A, 46, 433

[124] Wang, X., A. V. Filippenko, M. Ganeshalingam, et al., 2009, ApJL, 699, L139

[125] Wood-Vasey, W. M., G. Miknaitis, C. W. Stubbs, et al., 2007, ApJ, 666, 694

[126] Woosley, S. E., D. Kasen, S. Blinnikov, and E. Sorokina, 2007, ApJ, 662, 487

[127] Yip, C. W., A. J. Connolly, A. S. Szalay, et al., 2004, AJ, 128, 585

[128] Zheng, C., R. W. Romani, M. Sako, et al., 2008, AJ, 135, 1766